Article

Fine-tuning levels of filamins a and b as a specific mechanism sustaining Th2 lymphocyte functions

Kilian Maire [1], Léa Chamy[1], Samira Ghazali[1], Manon Carratala-Lasserre[1], Margot Zahm [1], Clément Bouisset [1], Arnaud Métais [2], Lucie Combes-Soia[2], Lidia de la Fuente-Vizuete[1], Hussein Trad[1], Adeline Chaubet [1], Magali Savignac[1], Anne Gonzalez de Peredo[2], Arun Subramaniam[3], Olivier Joffre [1], Pierre G. Lutz [1,4] ✉ & Isabelle Lamsoul [1,4] ✉

Augmenting the portfolio of therapeutics for type 2-driven diseases is crucial to address unmet clinical needs and to design personalized treatment schemes. An attractive therapy for such diseases would consist in targeting the recruitment of T helper 2 (Th2) lymphocytes to inflammatory sites. Herein, we show the degradation of filamins (FLN) a and b by the ASB2α E3 ubiquitin ligase as a mechanism sustaining Th2 lymphocyte functions. Low levels of FLNa and FLNb confer an elongated shape to Th2 lymphocytes associated with efficient $\alpha_V\beta_3$ integrin-dependent cell migration. Genes encoding the $\alpha_V\beta_3$ integrin and ASB2α belong to the core of Th2-specific genes. Using genetically modified mice, we find that increasing the levels of FLNa and FLNb in Th2 lymphocytes reduces airway inflammation through diminished Th2 lymphocyte recruitment in inflamed lungs. Collectively, our results highlight ASB2α and its substrates FLNa and FLNb to alter Th2 lymphocyte-mediated responses.

T helper (Th) lymphocytes are key mediators of adaptive immune responses that, via secretion of distinct cytokine combinations, orchestrate immune responses against foreign antigens, neo-antigens, and self-antigens, respectively in the context of infection, cancer, and auto-immunity. The understanding of the molecular mechanisms involved in the regulation of specific Th lymphocyte properties and functions will pave the way to the development of new approaches to tackle immune system-mediated diseases.

Asthma is a chronic inflammatory disease of the lower airways that affects nearly 400 million people worldwide. Despite the high diversity of endotypes characteristic of this pathology, half of asthmatic patients present a high type 2 inflammation initiated by the release of type 2 cytokines. Th2 lymphocytes represent a major source of type 2 cytokines and are key drivers of asthma pathogenesis because of their myriad effects on both structural and inflammatory cells in the airways[1,2]. Accordingly, many of the therapeutic antibodies for type 2-driven diseases are targeting type 2 cytokines and their receptors or IgE. In addition, a number of promising small-molecule drugs and vaccines are in the development pipeline[3]. Biologics have demonstrated encouraging results in clinical trials and some are approved for the type 2-high endotype of severe asthma[3,4]. These strategies may be further optimized when combined with the targeting of regulators of Th2 cell recruitment to sites of inflammation.

T cell migration is essential for T cell response[5]. The initial step usually happens in secondary lymphoid organs with the search for cognate antigen on many antigen-presenting cells that requires rapid scanning. Once activated and fully differentiated, effector T lymphocytes exit the lymph nodes and migrate to the site of injury in peripheral tissues to find their antigen. Motility of T lymphocytes is governed by cell-intrinsic events that are regulated by their activation

[1]Infinity, University of Toulouse, CNRS, Inserm, UPS, Toulouse, France. [2]Institut de Pharmacologie et de Biologie Structurale (IPBS), Université de Toulouse, CNRS, UPS, Toulouse, France. [3]Sanofi Immunology and Inflammation Research Therapeutic Area, Cambridge, MA, USA. [4]These authors jointly supervised this work: Pierre G. Lutz, Isabelle Lamsoul. ✉e-mail: Pierre.Lutz@inserm.fr; Isabelle.Lamsoul@inserm.fr

status as well as microenvironment cues. Beyond their distinct cytokine secretion profile, Th1 and Th2 lymphocytes harbor different scanning modes to migrate within inflamed tissues and optimize their respective effector functions[6,7]. In contrast to Th1 lymphocytes, Th2 lymphocytes appear to adopt a fast and wide scanning strategy that depends on $\alpha_V\beta_3$ integrins and is uncoupled from signals such as those triggered by chemokines[7].

Several E3 ubiquitin ligases are known to regulate differentiation and functions of Th2 lymphocytes[8,9]. Among them, ASB2α, the specificity subunit of a multimeric E3 ubiquitin ligase of the Cullin 5 RING Ligase (CRL5) family[10], is upregulated during Th2 differentiation of naive CD4^{+} T lymphocytes[11–13]. Importantly, loss of *ASB2* attenuated colitis-associated tumorigenesis in mice due to reduced Th2 response and enhanced type 1 antitumor immune response[13]. However, the molecular and cellular mechanisms whereby ASB2α exerts its effects to positively regulate Th2 lymphocyte function remain unknown. ASB2α triggers ubiquitylation and proteasomal degradation of filamins (FLN) a and b[14]. FLNa is an ubiquitously expressed actin-binding and cross-linking protein whose primary function is to organize actin filaments in an orthogonal network[15]. FLNa also interacts with about a hundred binding partners, many of which being involved in the regulation of signaling pathways converging towards actin cytoskeleton. Indeed, FLNa positively regulates signaling pathways downstream of the T cell receptor (TCR) and the CD28 costimulatory molecule[16–18] and interacts with Tc-mip (truncated c-MAF inducing protein), an adapter protein involved in c-MAF-dependent Th2 signaling pathway[19].

One of the most conserved activity of FLNa is to bind integrins, thereby maintaining the later in an inactive state[20]. Two mechanisms have been proposed. First, binding of FLNa to the C terminus of the integrin β tail (β_1, β_2, β_3, or β_7) results in direct competition with the binding of the integrin activator talin by occupying an overlapping binding site[21,22]. Second, FLNa can form a ternary complex engaging the cytoplasmic tails of both integrin α_{IIb} and β_3, thereby stabilizing the inner-membrane clasp and competing with talin recruitment to the β subunit cytoplasmic tail by binding both the C-terminal and membrane-proximal regions of the β_3 tail[23]. In addition, FLNa can also associate with the α_{IIb} cytoplasmic tail of active $\alpha_{IIb}\beta_3$ integrin to inhibit cell migration likely because of excessively enhanced integrin outside-in signaling[24]. We previously showed that ASB2α-mediated degradation of FLNa and FLNb regulates actin cytoskeleton remodeling and cell motility in different cell types[14,25–29]. However, the exact role and mechanisms of action of ASB2α in Th2 lymphocytes are not well-defined.

In the present study, we ask whether ASB2α triggers FLNa and FLNb degradation in Th2 lymphocytes and whether this is a mechanism sustaining Th2 lymphocyte functions. Furthermore, we investigate whether targeting the ASB2α-FLNa/b axis may represent a potential therapeutic opportunity in asthma using mouse models of airway inflammation. Using unbiased large-scale approaches, we show that FLNa and FLNb are the only substrates of ASB2α in Th2 lymphocytes and that low levels of FLNa and FLNb promote an elongated cell shape conducive to a dynamic migration. We further show that ASB2α-deficient Th2 lymphocytes exhibit less $\alpha_V\beta_3$ integrin-dependent dynamic behavior. Accordingly, loss of ASB2α in Th2 lymphocytes reduces their recruitment in inflamed lungs and attenuates airway inflammation.

Results

The actin-binding proteins FLNa and FLNb are substrates of ASB2α in Th2 lymphocytes

To elucidate the roles of ASB2α in Th2 lymphocytes, we first evaluated its expression in differentiating Th2 lymphocytes. ASB2α transcripts are highly upregulated after 5 days of culture of naive CD4^{+} lymphocytes in Th2 polarizing conditions (Fig. 1a) and are almost undetectable

in Th2 lymphocytes generated from *ASB2* cKO mice (Fig. 1b). Because E3 ubiquitin ligases often ubiquitylate several substrates, we used an unbiased and broad mass spectrometry approach to identify ASB2α substrates by comparing the whole proteomes of Th2 lymphocytes generated from ctrl or *ASB2* cKO mice. As expected, ASB2 peptides were barely detected in ASB2α-deficient Th2 lymphocytes (Fig. 1c, d). Deletion of *ASB2* had no impact on the expression of the master transcription factors of the Th2 lineage STAT6, GATA3, and c-MAF (Fig. 1d), suggesting no role of ASB2α in the generation of Th2 lymphocytes. Out of the >6400 quantified proteins in MS experiments, FLNa and FLNb stood out as the only proteins being more abundantly expressed in ASB2α-deficient vs ctrl Th2 lymphocytes (Fig. 1c, d and Supplementary Data 1 and Pride database with the dataset identifier PXD044062), pointing to the selectivity of ASB2α in controlling FLNa/FLNb levels. Enhanced expression of FLNa and FLNb at the protein levels in ASB2α-deficient Th2 lymphocytes was confirmed by western blot (Supplementary Fig. 1a) and intracellular flow cytometry (Fig. 1e). In contrast, levels of FLNa and FLNb transcripts were similar in ctrl and *ASB2* cKO Th2 lymphocytes (Supplementary Fig. 1b). Furthermore, we showed that FLNa was conjugated to ubiquitin chains in ctrl but not in *ASB2* cKO Th2 lymphocytes (Fig. 1f) and that FLNa degradation in ctrl Th2 lymphocytes was proteasome-dependent (Fig. 1g). Notably, lower levels of FLNa and FLNb in ctrl Th2 lymphocytes compared to naive CD4^{+} T lymphocytes or to other T effector lymphocytes were observed by western blot (Fig. 1h and Supplementary Fig. 1c) and by intracellular flow cytometry (Fig. 1i), while the levels of FLNa and FLNb transcripts were similar in Th1, Th2, Th17 and Treg lymphocytes (Supplementary Fig. 1d). In agreement with the low levels of ASB2α transcripts previously measured in naive CD4^{+} T lymphocytes, Th1 lymphocytes and Th17 lymphocytes[13], loss of ASB2α had no impact on the abundance of FLNa and FLNb in these cells (Supplementary Fig. 1e, f). Protein levels of FLNa were also lower in Th2 lymphocytes than in Th1 or Th17 lymphocytes of human peripheral blood mononuclear cells (PBMCs) isolated from healthy donors (Fig. 1j). ASB2α transcript and protein are also induced during in vitro Th2 differentiation of naive human CD4^{+} T lymphocytes (Fig. 1k, l and Supplementary Fig. 1g). In contrast, ASB2α transcripts are low in Th1 lymphocytes generated in vitro from naive human CD4^{+} T lymphocytes (Fig. 1k). Moreover, FLNa degradation in human Th2 lymphocytes is proteasome-dependent as evidenced by increased levels of FLNa after proteasome inhibition (Fig. 1m). Altogether, these results demonstrate that the FLNa and FLNb proteins are continuously and selectively degraded by ASB2α in mouse Th2 lymphocytes and suggest that this mechanism is conserved in humans.

Loss of ASB2α has no impact on the transcriptomic program of Th2 lymphocytes

Because ASB2α-mediated degradation of FLNa and FLNb could be involved in the modulation of Th2 lymphocyte signaling and thus in the regulation of Th2-specific genes, the transcriptomic signatures of ctrl and ASB2α-deficient Th2 lymphocytes were established by RNA-seq (Fig. 1n and Supplementary Fig. 2). Our analyses failed to detect differentially expressed genes between ctrl and *ASB2* cKO Th2 lymphocytes (Supplementary Data 2). In fact, Th2-specific genes exhibited similar expression patterns in ctrl and *ASB2* cKO Th2 lymphocytes, while Th1 and Th17 gene signatures were not deregulated in the absence of ASB2α (Supplementary Fig. 2a–d). Collectively, these analyses strongly support that ASB2α does not play a role in regulating the expression of Th genes. We next tested whether ASB2α-deficiency could nevertheless affect the transcriptional program in Th2 lymphocytes upon T-cell stimulation. Once again, our RNA-seq data did not reveal any significant difference between ctrl and *ASB2* cKO Th2 lymphocytes (Fig. 1n and Supplementary Fig. 2). Altogether, these data indicate that ASB2α does not shape Th2 lymphocyte identity at the transcriptional level.
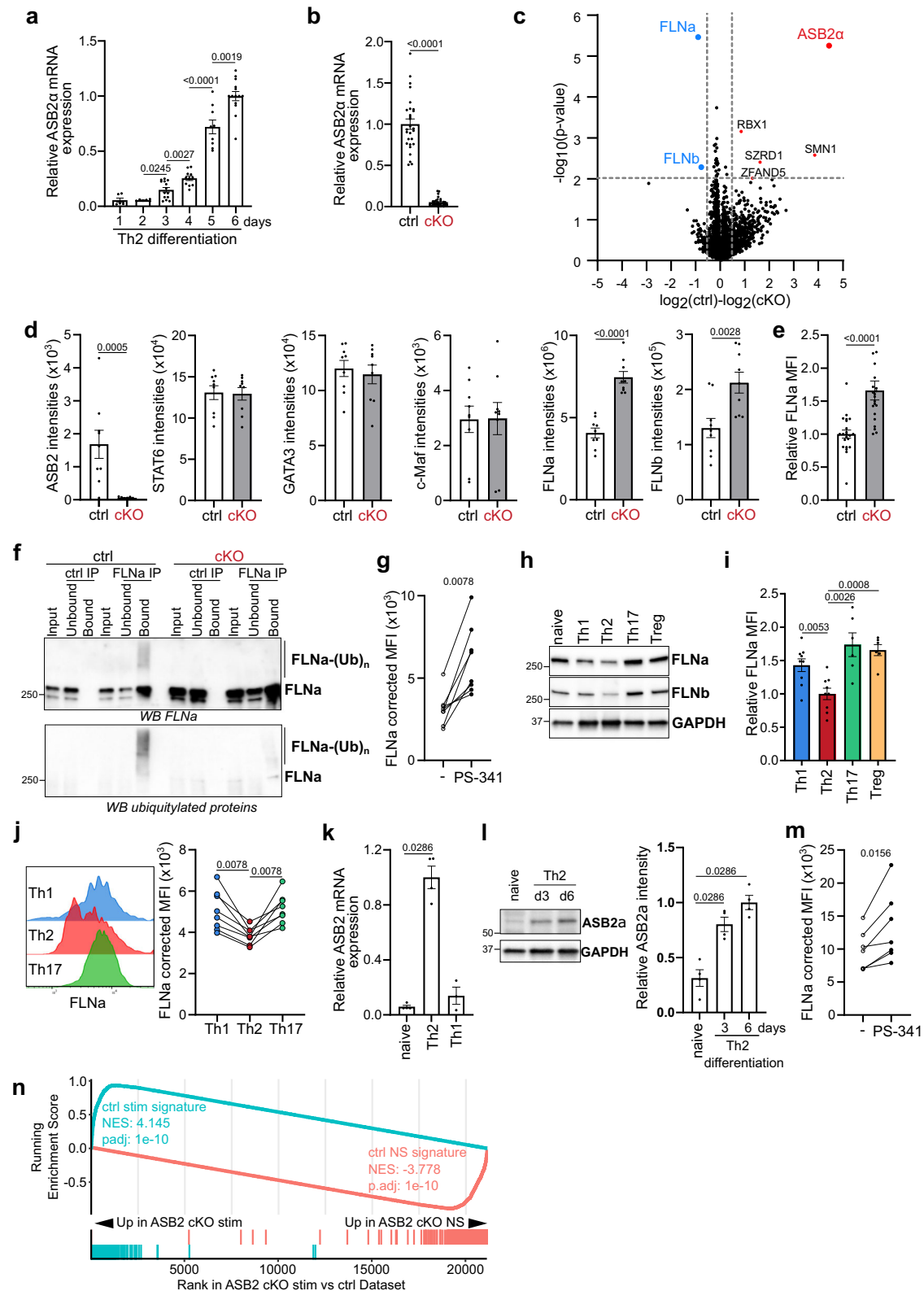
ASB2α-mediated degradation of FLNa and FLNb in Th2 lymphocytes correlates with specific morphological features

Because FLNa has a dual role in controlling the architecture and the mechanics of the actin cytoskeleton[20], we examined whether the lower levels of FLNa and FLNb in mouse Th2 lymphocytes impact cell morphology using high-content imaging. As shown in Fig. 2a–d, lower levels of FLNa and FLNb are associated with increased cell area and perimeter, as well as an elongated shape in Th2 lymphocytes compared to Th1, Th17, or Treg lymphocytes. In accordance with these observations, higher levels of FLNa and FLNb in ASB2α-deficient Th2 lymphocytes are associated with reduced cell area and perimeter, and a rounded shape of these cells compared to ctrl Th2 lymphocytes (Fig. 2e–g). In addition, low levels of FLNa in human Th2 lymphocytes are associated with increased cell area and perimeter, and an elongated shape compared to naive human CD4+ T lymphocytes (Fig. 2h, i). These results demonstrate that the low levels of FLNa and FLNb due to

Fig. 1 | FLNa and FLNb are substrates of ASB2α in mouse Th2 lymphocytes.
a Relative expression of ASB2α transcripts during Th2 differentiation of naive CD4⁺ T lymphocytes of ctrl mice assessed by RT-qPCR. **b** Expression of ASB2α transcripts in ctrl and *ASB2* cKO Th2 lymphocytes assessed by RT-qPCR. **c, d** Mass spectrometry quantitative analyses of protein abundance differences between cell extracts of ctrl and *ASB2* cKO Th2 lymphocytes. The volcano plot (**c**) illustrates for each protein the statistical significance of the variation as a function of the amplitude of the abundance (log2) difference between the two conditions. Dashed lines indicate cut-off values corresponding respectively to a Student *t*-test *p* value of 0.01 and a log2-transformed intensity difference of 0.5. Bar plots (**d**) show the intensities of ASB2, STAT6, GATA3, c-MAF, FLNa, and FLNb in each condition based on the MS measurements. Full data are presented in Supplementary Data 1. **e** Expression of FLNa was analyzed by intracellular flow cytometry in ctrl and *ASB2* cKO Th2 lymphocytes. **f** Cell extracts of ctrl and *ASB2* cKO Th2 lymphocytes were immunoprecipitated with control (Ctrl IP) or anti-FLNa (FLNa IP) antibodies. Pre-cleared cell lysates (input), unbound, and bound fractions were immunoblotted with antibodies to FLNa. After stripping, the blot was reprobed with antibodies to ubiquitylated proteins. One experiment out of two is shown. **g** Expression of FLNa was analyzed by intracellular flow cytometry in ctrl Th2 lymphocytes treated at day 5 with the PS-341 proteasome inhibitor at 4 nM during 20 h. **h** Expression of FLNa and FLNb was analyzed by western blot in naive CD4⁺ T cells, Th1, Th2, Th17, and Treg cells generated from naive CD4⁺ T lymphocytes of ctrl mice. **i** Expression of FLNa was analyzed by intracellular flow cytometry in Th1, Th2, Th17, and Treg cells generated from naive CD4⁺ T lymphocytes of ctrl mice. **j** Representative flow cytometry and quantification of FLNa expression in Th1 (CD4⁺CXCR3⁺CCR6⁻), Th2 (CD4⁺CXCR3⁻CCR6⁻CRTH2⁺) and Th17 (CD4⁺CXCR3⁻CCR6⁺) lymphocytes of human PBMCs. **k** Relative expression of ASB2 transcripts in naive human CD4⁺ T lymphocytes and after 5 days of culture in a Th2 or Th1 polarizing medium assessed by RT-qPCR. **l** Expression of ASB2α was analyzed by western blot in naive human CD4⁺ T lymphocytes and after 3 and 6 days of culture in a Th2 polarizing medium. **m** Expression of FLNa was analyzed by intracellular flow cytometry in human Th2 lymphocytes treated at day 5 with the PS-341 proteasome inhibitor at 10 nM during 20 h. **n** Gene set enrichment analyses of genes significantly up- and down-regulated in ctrl Th2 lymphocytes upon stimulation performed using transcriptomes of stimulated *vs* non-stimulated *ASB2* cKO Th2 lymphocytes. Data are mean ± SEM of biological replicates. Sample size, d1 = 6, d2 = 6, d3 = 14, d4 = 11, d5 = 9 and d6 = 14 for (**a**); ctrl = 28 and cKO = 32 for (**b**); ctrl = 9 and cKO = 9 for (**c**); ctrl = 9 and cKO = 9 for (**d**); ctrl = 22 and cKO = 21 for (**e**); ctrl = 8 for (**g**); Th1 = 9, Th2 = 9, Th17 = 6 and Treg = 6 for (**i**); *n* = 8 for (**j**); naive = 4, Th2 = 4 and Th1 = 3 for (**k**); *n* = 4 for (**l**); and *n* = 7 for (**m**). *p* values were calculated using the two-sided Mann−Whitney *t*-test except in (**g**, **j**, **m**) where the Wilcoxon matched-pairs signed rank test was used. Source data are provided as a Source Data file.

their degradation driven by ASB2α confer specific morphological features to Th2 lymphocytes.

### *ASB2*, *ITGAV* and *ITGB3* belong to the core of Th2-specific genes

Because FLNa is also a gatekeeper to integrin activation[20], we next examined the expression of α and β integrin subunits in Th2 lymphocytes by semi-quantitative MS. As shown in Fig. 3a and Supplementary Data 1, the αᵥβ₃ integrin together with the leukocyte-specific αᵢβ₂ integrin are the main integrin proteins expressed in Th2 lymphocytes and *ASB2* deficiency has no impact on their abundance. Given that transcriptional specificity is largely controlled by chromatin-based regulations in differentiating Th cells, we hypothesized that the genes encoding the αᵥ (*ITGAV*) and β₃ (*ITGB3*) integrin subunits and the ASB2α protein might be differentially controlled by epigenetic regulatory pathways in different Th cell lineages. We first conducted expression profiling of genes encoding the α and β subunits of integrins in naive, Th1, Th2, and Th17 lymphocytes using our previously published transcriptomic data[30]. ASB2, ITGAV, and ITGB3 transcripts are more expressed in Th2 lymphocytes compared to in naive, Th1, and Th17 lymphocytes (Fig. 3b). Global mapping of RNApol II, and active (H3K27ac, H3K4me1) and repressive (H3K27me3) histone marks in naive, Th1, Th2 and Th17 lymphocytes indicated that *ASB2*, *ITGAV* and *ITGB3* genes harbor cis-regulatory regions that are specifically active in Th2 lymphocytes. These latter are either poised or repressed through H3K27me3-dependent silencing mechanisms in the other lineages (Fig. 3c). This indicates that chromatin remodeling machineries maintain these enhancers in their respective active and silent states implying that these three genes play an important role in Th2 lymphocyte identity and/or function. All these data imply that *ASB2*, *ITGAV*, and *ITGB3* belong to the core of Th2-specific genes. We then wondered whether the expression of ASB2, ITGAV, and ITGB3 transcripts were upregulated in Th2 lymphocyte-dependent pathological settings. Analyses of transcriptomic data[31,32] showed that ASB2, ITGAV, and ITGB3 transcripts are upregulated in both ovalbumin (OVA)-induced airway inflammation and house dust mite (HDM)-induced asthma (Supplementary Fig. 3a, b). Importantly, cell surface expression of αᵥ and β₃ integrin subunits was also higher in human Th2 lymphocytes compared to naive CD4⁺ T lymphocytes or Th1, Th17 and Treg lymphocytes of human PBMCs (Fig. 3d), and in vitro generated human Th2 lymphocytes compared to naive human CD4 + T lymphocytes (Fig. 3e). Overall, these results indicate a coordinated regulation of ASB2α and αᵥβ₃ integrin in Th2 lymphocytes to build an efficient Th2 lymphocyte response.

ASB2α-mediated degradation of FLNa and FLNb regulates migration properties of Th2 lymphocytes

FLNa is a negative regulator of integrin-dependent cell migration[21,23,24]. We, therefore, speculated that degradation of FLNa and FLNb triggered by ASB2α in Th2 lymphocytes favors fast αᵥβ₃ integrin-dependent migration. We first verified that ASB2α loss has no effect on the total amount and cell surface expression of αᵥ and β₃ integrin subunits (Fig. 3a and Supplementary Fig. 3c–e). We then used live imaging to study the dynamics of ctrl and *ASB2* cKO Th2 lymphocytes seeded onto vitronectin-coated slides (Supplementary Movies 1, 2). Single-cell analysis revealed marked differences in the dynamic motility patterns of ctrl and *ASB2* cKO Th2 lymphocytes (Fig. 4a–f). ASB2α-deficient Th2 lymphocytes exhibited a diminished track displacement length (Fig. 4a, c), a diminished mean scanned area and persistence (Fig. 4a, d, e), associated with a reduced cell velocity compared to ctrl Th2 lymphocytes (Fig. 4f, left panel). This reduced cell velocity is not due to a defect in the initiation of the migration since cells that have a track length > 50 μm present also a reduced velocity in the absence of *ASB2* (Fig. 4f, right panel). Our results demonstrated that ASB2α-deficient Th2 lymphocytes are less motile, indicating that loss of ASB2α impacted the dynamic behavior of Th2 lymphocytes. As previously observed with fixed cells, live imaging showed that ASB2α-deficient Th2 lymphocytes have a rounded shape compared to ctrl Th2 lymphocytes (Fig. 4g). Moreover, we observed a positive correlation between the elongated shape and the track displacement length or the average velocity of ctrl Th2 lymphocytes but not of ASB2α-deficient Th2 lymphocytes (Fig. 4h, i). Taken together, our data demonstrate that the low levels of FLNa and FLNb due to their degradation driven by ASB2α confer specific migratory properties to Th2 lymphocytes.

Accumulation of FLNa and FLNb inhibits αᵥβ₃ integrin-dependent migration of ASB2α-deficient Th2 lymphocytes by enhancing integrin activation

To understand how FLNa and FLNb accumulation in ASB2α-deficient Th2 lymphocytes inhibits cell migration, we challenged the two models linking FLNa to inhibition of integrin-dependent cell motility. In the first model, FLNa maintains integrins in an inactive state[21]. In a second model, FLNa promotes integrin outside-in signaling leading to inhibition of dynamic cell movement[24]. We first studied by live imaging the dynamics of ctrl and *ASB2* cKO Th2 lymphocytes treated with MnCl₂ to activate integrins and allowed to migrate onto vitronectin-coated slides. Compared to untreated ctrl Th2 lymphocytes, MnCl₂-treated ctrl Th2 lymphocytes exhibited a diminished track displacement length and a reduced cell velocity that were similar to those measured
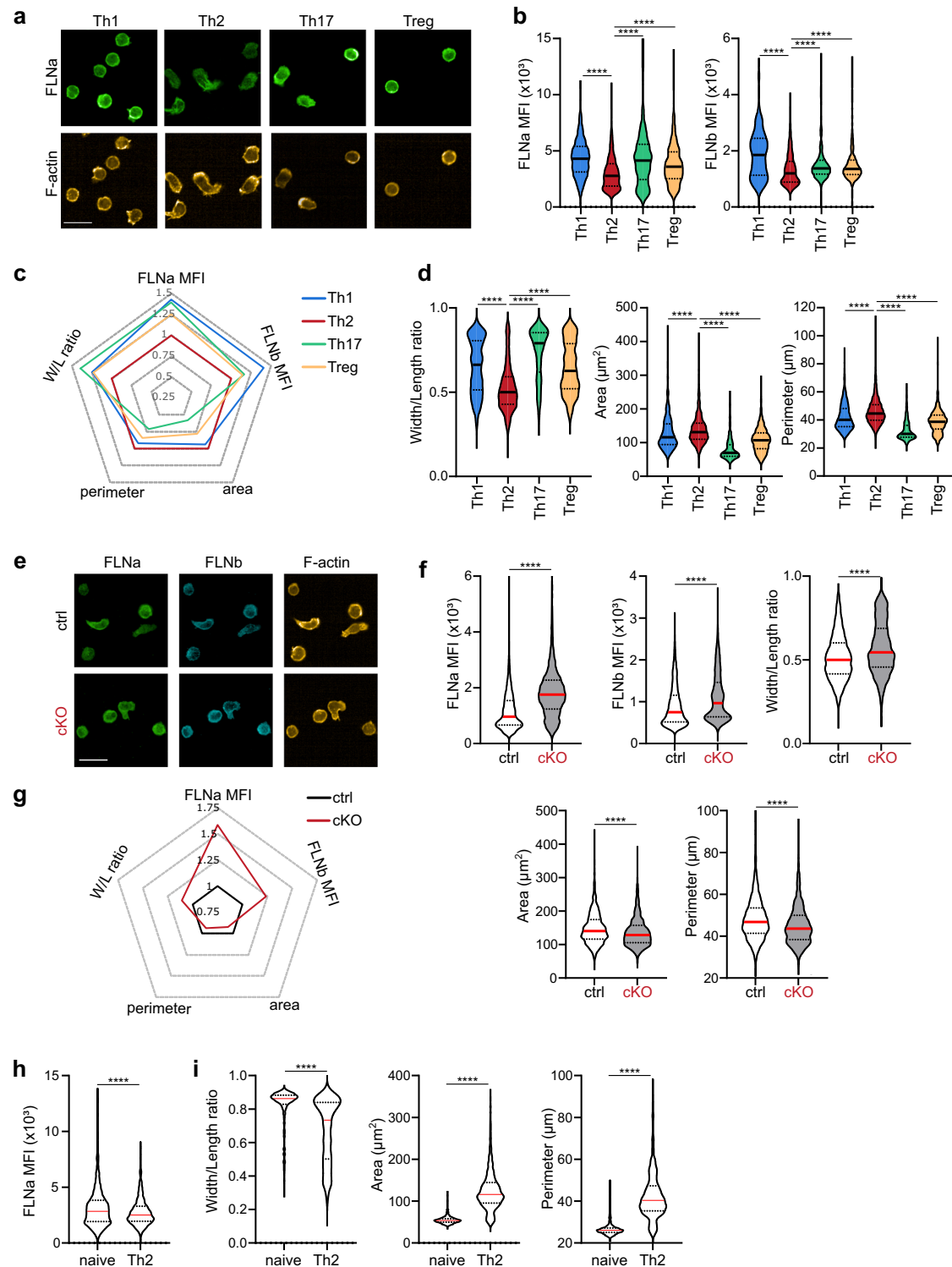
in untreated or in MnCl$_2$-treated *ASB2* cKO Th2 lymphocytes (Supplementary Movi*es* 3–6 and Fig. 5a–d), suggesting that integrins are more activated in ASB2α-deficient Th2 lymphocytes than in ctrl Th2 lymphocytes. We then assessed the dynamics of ctrl and *ASB2* cKO Th2 lymphocytes treated with a combination of anti-α$_V$ and anti-β$_3$ integrin blocking antibodies to inhibit integrins. As expected, following α$_V$β$_3$ integrin inhibition, ctrl Th2 lymphocytes showed decreased track displacement length and decreased cell velocity compared to untreated cells in agreement with the role of the α$_V$β$_3$ integrin in Th2 lymphocyte migration cells (Supplementary Movies 7, 8 and Fig. 5e–h). In contrast, following α$_V$β$_3$ integrin inhibition, *ASB2* cKO Th2

lymphocytes exhibited an enhanced track displacement length and an increased cell velocity compared to untreated cells (Supplementary Movi*es* 9, 10 and Fig. 5e–h), reinforcing the view that increased levels of FLNa and FLNb in *ASB2* cKO Th2 lymphocytes leads to abnormal α$_V$β$_3$ integrin-dependent cell migration.

Deletion of *ASB2* in hematopoietic cells attenuates OVA-induced airway inflammation and HDM-induced asthma

We next investigated the specific role of ASB2α in Th2 lymphocytes in a mouse model of airway inflammation. Compared to ctrl mice, induction of airway inflammation with OVA injection and challenge in *ASB2*

Fig. 2 | ASB2α-mediated degradation of FLNa and FLNb confers specific morphological features to Th2 lymphocytes. a–d Th1, Th2, Th17, and Treg ctrl lymphocytes were seeded onto VCAM-1 coated 384-well plates and analyzed by immunofluorescence with antibodies to FLNa and FLNb or phalloidin. Representative fluorescent images of one experiment out of 3 (**a**), FLNa MFI and FLNb MFI (**b**), radar plot with FLNa MFI, FLNb MFI, cell area, cell perimeter, and width to length ratio (relative to the values measured in Th2 lymphocytes) (**c**) and violin plots of cell area, cell perimeter and width to length ratio (**d**) are shown. **e–g** Ctrl and *ASB2* cKO Th2 lymphocytes were allowed to adhere in 384-well plates coated with vitronectin, fixed, and stained for FLNa, FLNb, and F-actin. Representative fluorescent images of one experiment out of 4 (**e**), radar plot with FLNa MFI, FLNb MFI, cell area, cell perimeter, and width-to-length ratio (relative to the values measured in ctrl Th2 lymphocytes) (**f**), and violin plots with FLNa MFI, FLNb MFI, cell area, cell perimeter and width to length ratio (**g**) are shown. **h, i** Human naive CD4 + T lymphocytes and in vitro generated Th2 lymphocytes were seeded onto VCAM-1 coated 384-well plates and analyzed by immunofluorescence with antibodies to FLNa or phalloidin. Violin plots of FLNa MFI (**h**), cell area, cell perimeter, and width-to-length ratio (**i**) are shown. Scale bar, 20 μm. Data are mean ± SEM. Sample size: Th1 = 2097, Th2 = 3397, Th17 = 1284 and Treg = 1918 for (**b**) (*left*); Th1 = 222, Th2 = 660, Th17 = 750 and Treg = 951 for (**b**) (*right*); Th1 = 1002, Th2 = 2405, Th17 = 486 and Treg = 560 for (**d**) (*left*); ctrl = 7189 and cKO = 6878 for (**f**) (*FLNa MFI*); ctrl = 5159 and cKO = 3139 for (**f**) (*FLNb MFI*); ctrl = 2589 and cKO = 1605 for (**f**) (*width/length ratio, area, perimeter*); naive = 1141 and Th2 = 1137 for **i**. *p* values were calculated using the two-sided Mann–Whitney *t*-test except in (**g, j**) where the Wilcoxon matched-pairs signed rank test was used. Source data are provided as a Source Data file.

cKO mice resulted in: (i) decreased cell infiltration determined by histological score after hematoxylin and eosin (HE) staining of lung sections, decreased mucus secretion assessed by the percentage of Periodic Acid Schiff (PAS) positive bronchi after PAS staining of lung sections and decreased remodeling of the airways quantified by collagen deposits after Masson's trichrome (MT) staining of lung sections (Fig. 6a); (ii) reduced numbers of leukocytes in the lungs (Fig. 6b); (iii) reduced percentages but similar numbers of alveolar macrophages (Fig. 6c), (iv) less eosinophil recruitment in the lungs (Fig. 6c) in agreement with the reduced expression of eotaxin 2 mRNA in lung lysates (Fig. 6d); (v) reduced numbers of CD4+ cells and Th2 lymphocytes in the lungs (Fig. 6e, f); (vi) similar percentages of CD4+ cells and reduced percentages of Th2 lymphocytes in the bronchoalveolar lavage fluids (BALF; Fig. 6g); (vi) decreased mRNA levels of IL-4, IL-5 and IL-13 in lung lysates (Fig. 6h); (vii) reduced percentages of IL-4+, IL-5+ or IL-13+ in CD4+ cells in the lungs and reduced percentages of IL-4+, IL-5+ or IL-13+ in ST2+CD4+ cells in the lungs (Fig. 6i); and (viii) reduced IL-4, IL-5 and IL-13 secretion by LDLN cells after OVA-antigen restimulation (Fig. 6j). In contrast, numbers and percentages of Th1 lymphocytes in the lungs as well as mRNA levels of TBX21 and IFNG were similar in ctrl and *ASB2* cKO mice submitted to OVA-induced inflammation (Supplementary Fig. 4), indicating comparable Th1 responses. FLNa is a substrate for ASB2α in lung-infiltrating Th2 lymphocytes of mice submitted to OVA-airway inflammation as evidenced by increased FLNa intensity in *ASB2* cKO mice measured by intracellular flow cytometry (Fig. 6k) or mass spectrometry (Fig. 6l). We also used a more clinically-relevant asthma model based on repeated exposures to HDM inhalation. As shown in Fig. 7, loss of ASB2α resulted in: (i) decreased inflammation and mucus production (Fig. 7a); (ii) decreased recruitment of leukocytes in the inflamed lungs (Fig. 7b); (iii) decreased recruitment of eosinophils in the lungs (Fig. 7c) and in BALF (Fig. 7d); (iv) similar numbers of CD4+ cells and decreased recruitment of Th2 lymphocytes in the lungs (Fig. 7e); and (v) similar percentages of CD4+ cells in leukocytes and reduced percentages of ST2+ cells in CD4+ T cells in the BALF (Fig. 7f). Furthermore, intracellular flow cytometry experiments showed that FLNa is more abundant in ASB2α-deficient vs ctrl Th2 lymphocytes from the lungs of mice submitted to HDM-asthma indicating that FLNa is also a substrate of ASB2α in Th2 lymphocytes in vivo in a clinically-relevant asthma model (Fig. 7g). Collectively, our results show that loss of ASB2α in hematopoietic cells decreases airway inflammation in both models.

## ASB2α expressed by Th2 lymphocytes is key to the mediation of airway inflammation

To evaluate whether ASB2α in Th2 lymphocytes plays important roles in airway inflammation, we used a mouse model that relies on the adoptive transfer of ctrl or *ASB2* cKO OVA-specific (OT2) Th2 lymphocytes to C57Bl/6 recipients followed by OVA inhalation. Deletion of *ASB2* decreased cell infiltration, mucus secretion, and remodeling of the airways (Fig. 7h–j). Compared to mice that received ctrl OT2 Th2 lymphocytes, mice that received *ASB2* cKO OT2 Th2 lymphocytes

showed: (i) reduced leukocyte infiltration in the lungs (Fig. 7k); (ii) reduced frequencies and reduced numbers of eosinophils in the lungs (Fig. 7l); (iii) reduced frequencies of eosinophils in the BALF (Fig. 7m); (iii) reduced numbers of Vβ5+Vα2+CD4+CD45+ cells in the lungs (Fig. 7n); (iv) reduced frequencies of OT2 Th2 lymphocytes in the lungs and BALF (Fig. 7o). Altogether, our results indicate that ASB2α expressed by Th2 lymphocytes is key to the mediation of airway inflammation and point to ASB2α-mediated degradation of FLNa and FLNb as a molecular mechanism sustaining Th2 lymphocyte functions. To further elucidate how ASB2α loss and subsequent accumulation of FLNa and FLNb alters Th2 lymphocyte functions leading to attenuated airway inflammation, we analyzed the recruitment of transferred OT2 Th2 lymphocytes into the lungs 24 h after the first OVA inhalation. The numbers of *ASB2* cKO OT2 Th2 lymphocytes in the lungs (Fig. 7p) and their frequencies in the lungs and BALF (Fig. 7q) were lower compared to those of ctrl Th2 lymphocytes, suggesting decreased recruitment of ASB2α-deficient Th2 lymphocytes in the inflamed area. Taken together, our results demonstrate that loss of ASB2α in Th2 lymphocytes reduces cell mobility and attenuates the recruitment of Th2 lymphocytes in inflamed areas, suggesting that increasing levels of FLNa and FLNb in Th2 lymphocytes might mitigate pathogenic type 2 immune responses.

Discussion

In this study, we identified original targets to rewire Th2 lymphocyte-mediated responses. We revealed an unexpected role for ASB2α-mediated degradation of FLNa and FLNb in Th2 lymphocyte-specific functions and properties, and therefore in airway inflammation. Using genetically modified mice, we found that increasing the levels of FLNa and FLNb in Th2 lymphocytes attenuates airway inflammation. Collectively, our results highlight the ASB2α-FLNa/b axis as a potential therapeutic opportunity to rewire Th2 lymphocyte-mediated responses.

T lymphocytes are essential for adaptive immune responses, in particular CD4+ lymphocytes, which differentiate into effector T lymphocyte subtypes depending on environmental cues. This is largely achieved through transcription factors and chromatin remodelers that initiate and maintain a heritable gene expression program. Indeed, they positively regulate genes critical to the functions one specific Th subset while repressing genes controlling the functions of the other subsets. *ASB2*, *ITGAV* and *ITGB3* belong to the core set of Th2-specific genes that share common mechanisms of epigenetic and play essential roles in the establishment of the Th2 lymphocyte identity and/or in Th2 lymphocyte functions[33–35]: (i) transcripts of ASB2α, ITGAV and ITGB3 are higher in the Th2 subset of CD4+ T lymphocytes compared to in naive or to in other Th lymphocytes[13,33,36] (and data herein); (ii) active marks were associated with the *ASB2*, *ITGAV* and *ITGB3* loci in Th2 lymphocytes; (iii) *ASB2*, *ITGAV* and *ITGB3* are upregulated in both OVA-induced airway inflammation and HDM-induced asthma[31,32,37,38]. Furthermore, high expression of *ITGAV* and *ITGB3* transcripts in mouse Th2 lymphocytes correlated with high levels of the αVβ3 integrin
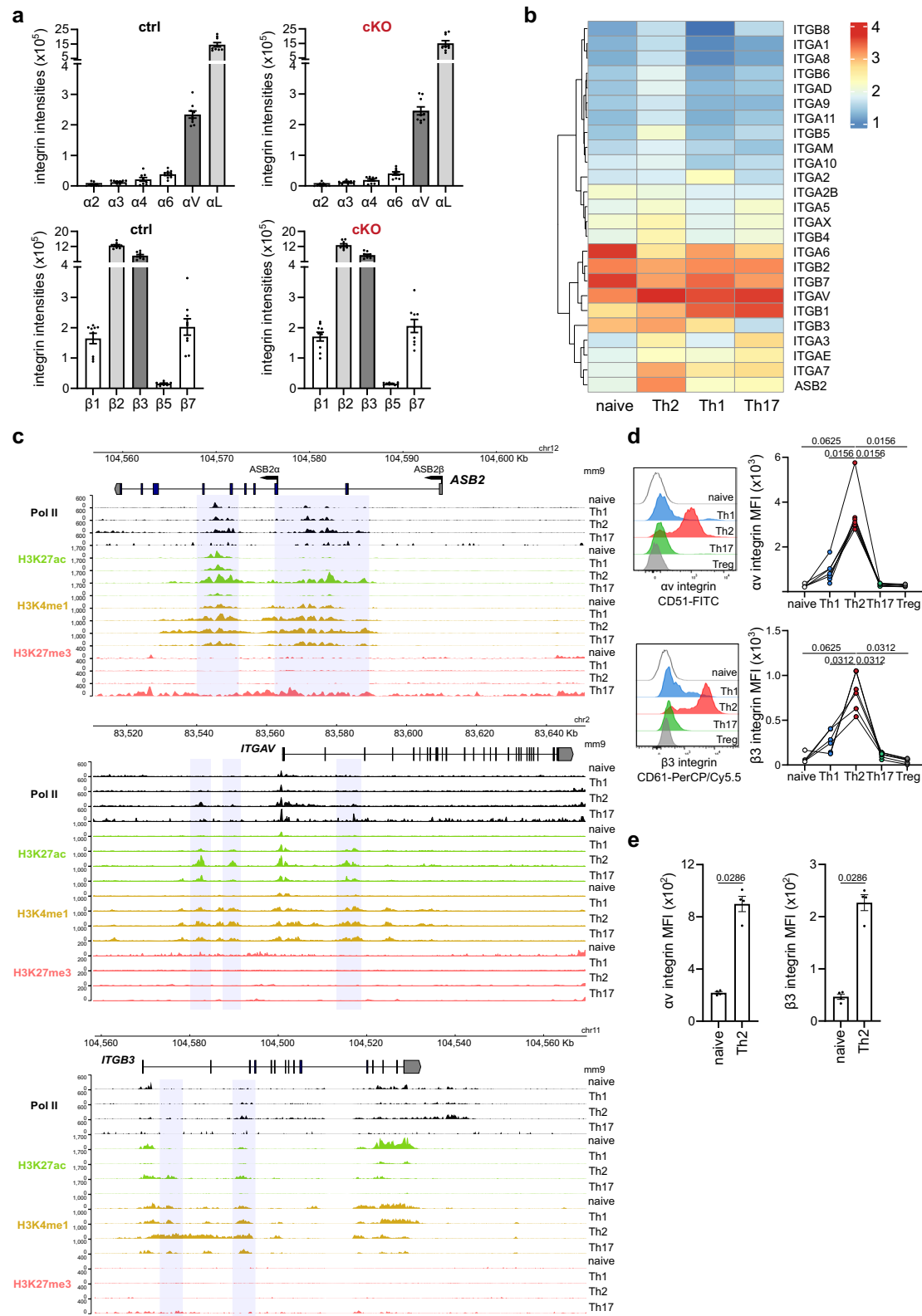
protein (data herein and[7]). Importantly, higher expression of α_V and β_3 integrin subunits in Th2 lymphocytes compared to the other Th subsets is conserved between humans and mice (data herein and[7,39]). Because Th2-specific genes including those encoding type 2 cytokines exhibited similar expression patterns in ctrl and ASB2α-deficient Th2 lymphocytes, the mechanisms linking Thy1-$\alpha_V\beta_3$ integrin interactions to enhanced Th2 lymphocyte differentiation and increased IL-13/IL-5 production[39] is unlikely to rely on the abundance of FLNa and FLNb.

Taken together, these reinforce the view that the $\alpha_V\beta_3$ integrin is critical to Th2 specific functions and antigen-specific lung Th2 lymphocyte responses[7,39].

Asthma is characterized by an exacerbated Th2 lymphocyte-mediated inflammation. Herein, we demonstrate that the loss of the *ASB2* gene in hematopoietic cells attenuates OVA-induced airway inflammation and HDM-induced asthma in mice. Although we do not exclude the contribution of other immune cells that would be affected

Fig. 3 | *ASB2*, *ITGAV*, and *ITGB3* are Th2-specific genes. a Mass spectrometry semi-quantitative analyses of integrin abundance in cell extracts of ctrl and *ASB2* cKO Th2 lymphocytes (*n* = 9 replicates). Full data are presented in Supplementary Data 1. **b** Heatmap showing the expression of genes encoding the α and β integrin subunits (ITGA and ITGB, respectively) in naive, Th2, Th1, and Th17 cells (analyzed from ref. [30]). RPKM intensities were log10 transformed and are displayed as colors ranging from blue to red as shown in the key. **c** RNA polymerase II (Pol II), H3K27ac, H3K4me1 and H3K27me3 signals across the *ASB2, ITGAV and ITGB3* loci. The identified *cis*-regulatory regions are highlighted (GSE144586[30]); **d** Representative flow cytometry and quantification of cell surface expression of α$_V$ and β$_3$ integrin

subunits in naive CD4$^+$ T cells and in Th1 (CD4$^+$CXCR3$^+$CCR6$^-$CRTH2$^-$FoxP3$^-$), Th2 (CD4$^+$CXCR3$^-$CCR6$^-$CRTH2$^+$FoxP3$^-$), Th17 (CD4$^+$CXCR3$^-$CCR6$^+$CRTH2$^-$FoxP3$^-$) and Treg (CD4$^+$CXCR3$^-$CCR6$^-$CRTH2$^-$FoxP3$^+$) lymphocytes of human PBMCs. **e** Quantification of cell surface expression of α$_V$ and β$_3$ integrin subunits in naive and in vitro generated human Th2 lymphocytes. Data are mean ± SEM of biological replicates. Sample size: ctrl = 9 and cKO = 9 for (**a**); *n* = 6 for (**d**); and *n* = 4 for (**e**). *p* values were calculated using the two-sided Mann–Whitney *t*-test except in (**d**) where the Wilcoxon matched-pairs signed rank test was used. Source data are provided as a Source Data file.
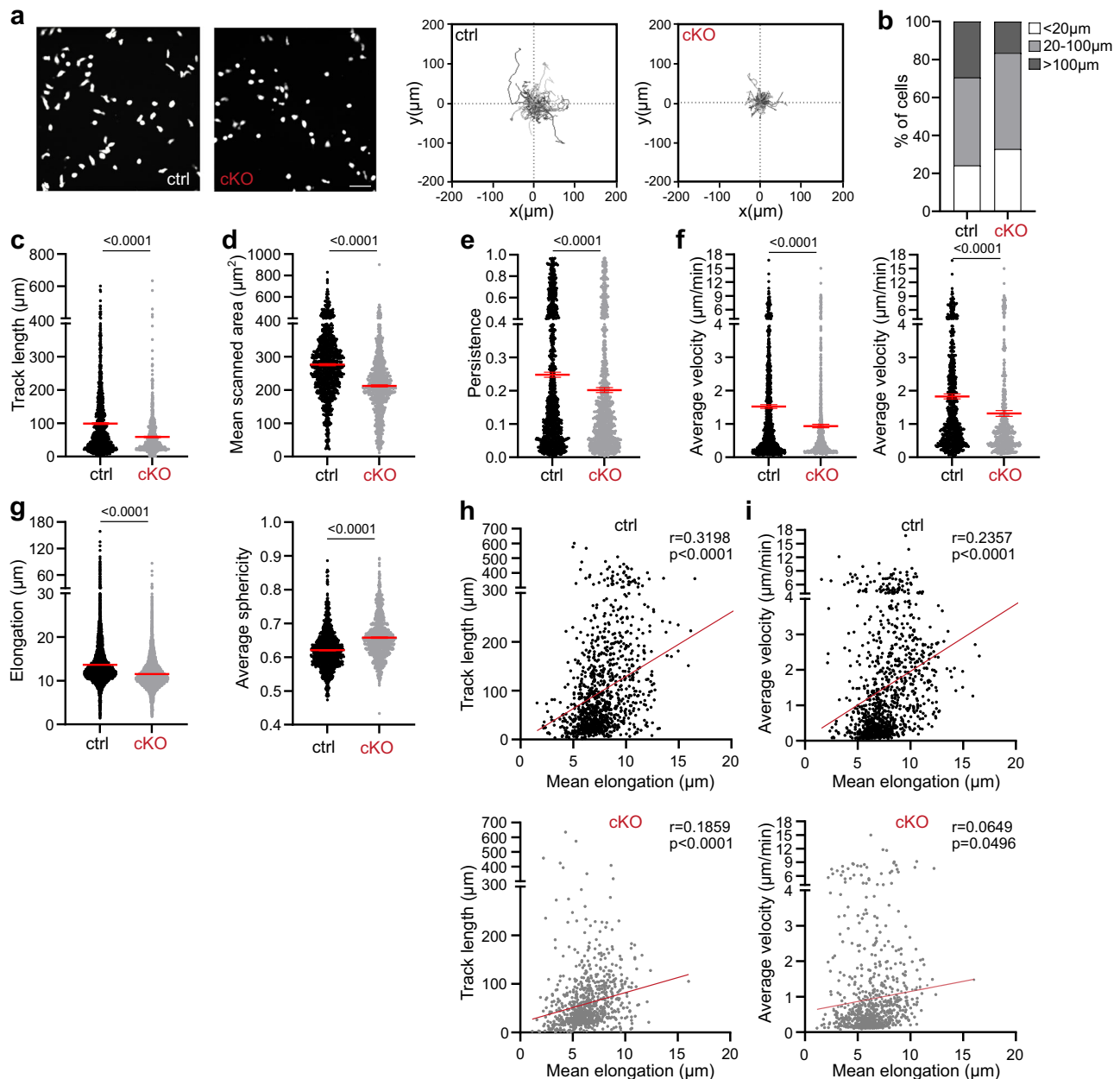

Fig. 4 | ASB2α-mediated degradation of FLNa and FLNb confers specific migration properties to Th2 lymphocytes. Ctrl and *ASB2* cKO Th2 lymphocytes seeded onto vitronectin-coated slides were imaged by time-lapse microscopy. Representative images (left) and individual tracks (right) of one experiment out of 5 (**a**), percentages of migrating cells (**b**), track length (**c**), mean scanned area (**d**), persistence coefficient (**e**), average velocities of all the cells (left panel) or cells with a track length > 50 μm (right panel) (**f**), elongation coefficient and average sphericity (**g**) are shown. Scatter plots showing correlation data for elongation coefficient and track length (**h**) or average velocity (**i**) of ctrl or *ASB2* cKO Th2 lymphocytes.

Linear regression-fit curves are shown as red lines. Scale bar, 20 μm. In (**a–g**), Data are mean ± SEM of 5 biological replicates. Sample size: ctrl = 1070 and cKO = 916 for (**c**); ctrl = 1070 and cKO = 916 for (**d**); ctrl = 1070 and cKO = 916 for (**e**); ctrl = 1070 and cKO = 916 for (**f**) (*left*); ctrl = 685 and cKO = 470 for (**f**) (*right*); ctrl = 92,674 and cKO = 85,399 for (**g**); ctrl = 1070 and cKO = 916 for (**h**); and ctrl = 1070 and cKO = 916 for (**i**). *p* values were calculated using the two-sided Mann–Whitney *t*-test. In (**h**, **i**), correlations between nonparametric variables were evaluated using Spearman rank correlation test (*r*). Source data are provided as a Source Data file.
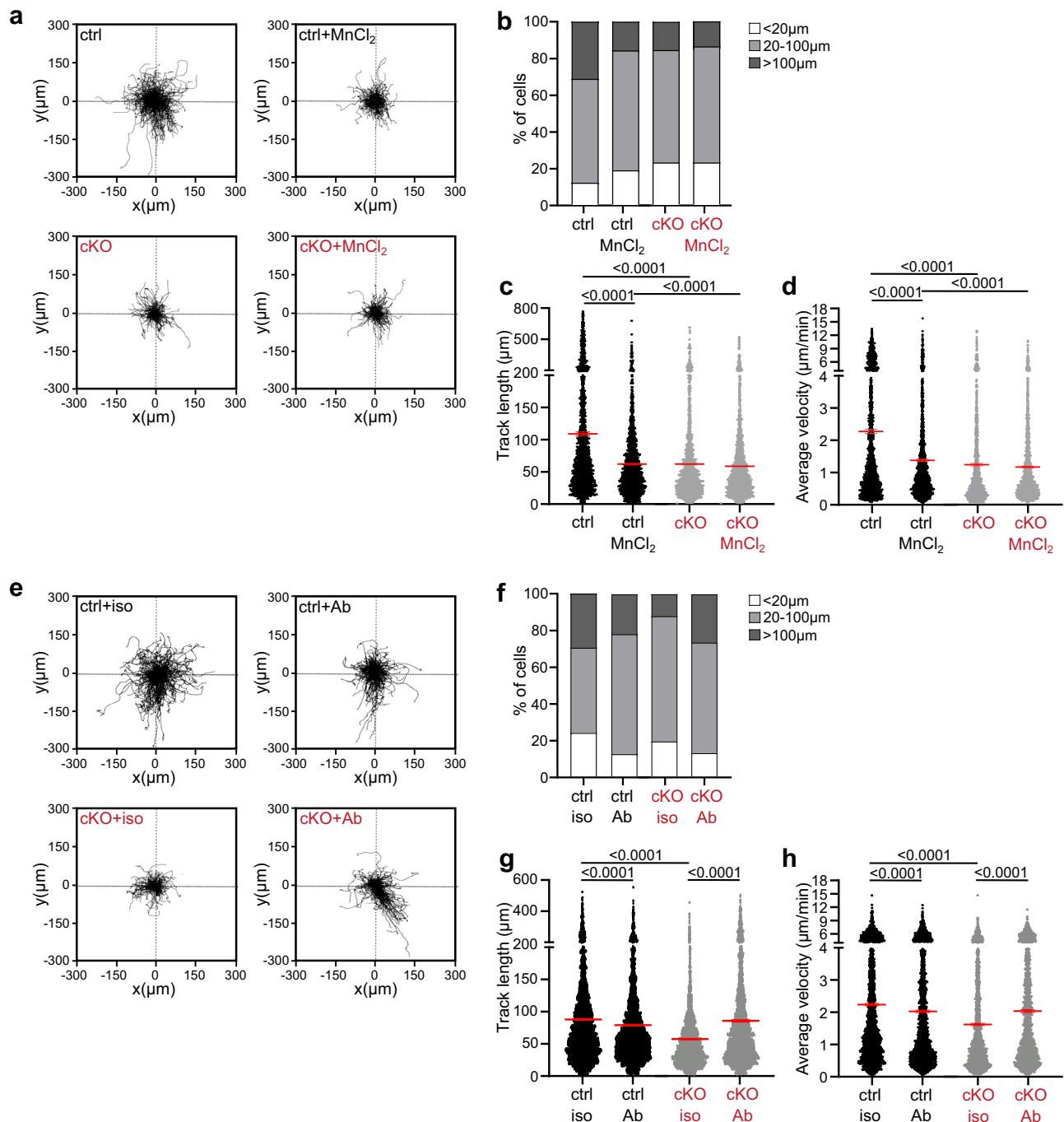
Fig. 5 | Migration properties of ctrl and *ASB2* cKO Th2 lymphocytes following MnCl$_2$-induced integrin activation or $\alpha_v\beta_3$ inhibition. Ctrl and *ASB2* cKO Th2 lymphocytes were either untreated or treated with MnCl$_2$ (**a**–**d**) and treated with anti-α_v and anti-β_3 integrin blocking antibodies (Ab) or their corresponding isotypic controls (iso) (**e**–**h**), and allowed to migrate onto vitronectin-coated slides. Cells were imaged by time-lapse microscopy. Individual tracks (**a**, **e**), percentages of migrating cells (**b**, **f**), track length (**c**, **g**), average velocities of all the cells (**d**, **h**) are shown. Data are mean ± SEM of 4 and 5 biological replicates for ctrl and cKO Th2 lymphocytes respectively. Sample size: ctrl = 1809, ctrl+MnCl$_2$ = 2344, cKO = 1611, and cKO + MnCl$_2$ = 1717 for (**c**, **d**); and ctrl + iso = 2768, ctrl +Ab = 2803, cKO + iso = 2261, and cKO + Ab = 1989 for (**g**, **h**). *p* values were calculated using the two-sided Mann–Whitney *t*-test. Source data are provided as a Source Data file.

by *ASB2* deficiency, we show that Th2 lymphocytes play a major contributing role to the impact of *ASB2* deletion on airway inflammation using a passive airway inflammation mouse model that relies on the adoptive transfer of OVA-specific Th2 lymphocytes followed by OVA-inhalation.

Our large-scale protein expression profiling based on quantitative mass spectrometry analysis shows that only FLNa and FLNb accumulated in *ASB2* cKO Th2 lymphocytes. We also observed polyubiquitylation of FLNa in ctrl Th2 lymphocytes but not in *ASB2* cKO

Th2 lymphocytes, accumulation of FLNa in ctrl Th2 lymphocytes treated with the PS-341 proteasome inhibitor as well as accumulation of FLNa in Th2 lymphocytes of the lungs of *ASB2* cKO mice submitted to OVA-induced airway inflammation or HDM-induced asthma. All these results demonstrate that FLNa and FLNb are continuously targeted to proteasomal degradation by the ASB2α CRL5 in Th2 lymphocytes as previously shown in other cell types[14,25,29], and point out to the high selectivity of ASB2α towards FLNa and FLNb. Although FLNa was previously shown to regulate signaling pathways downstream of
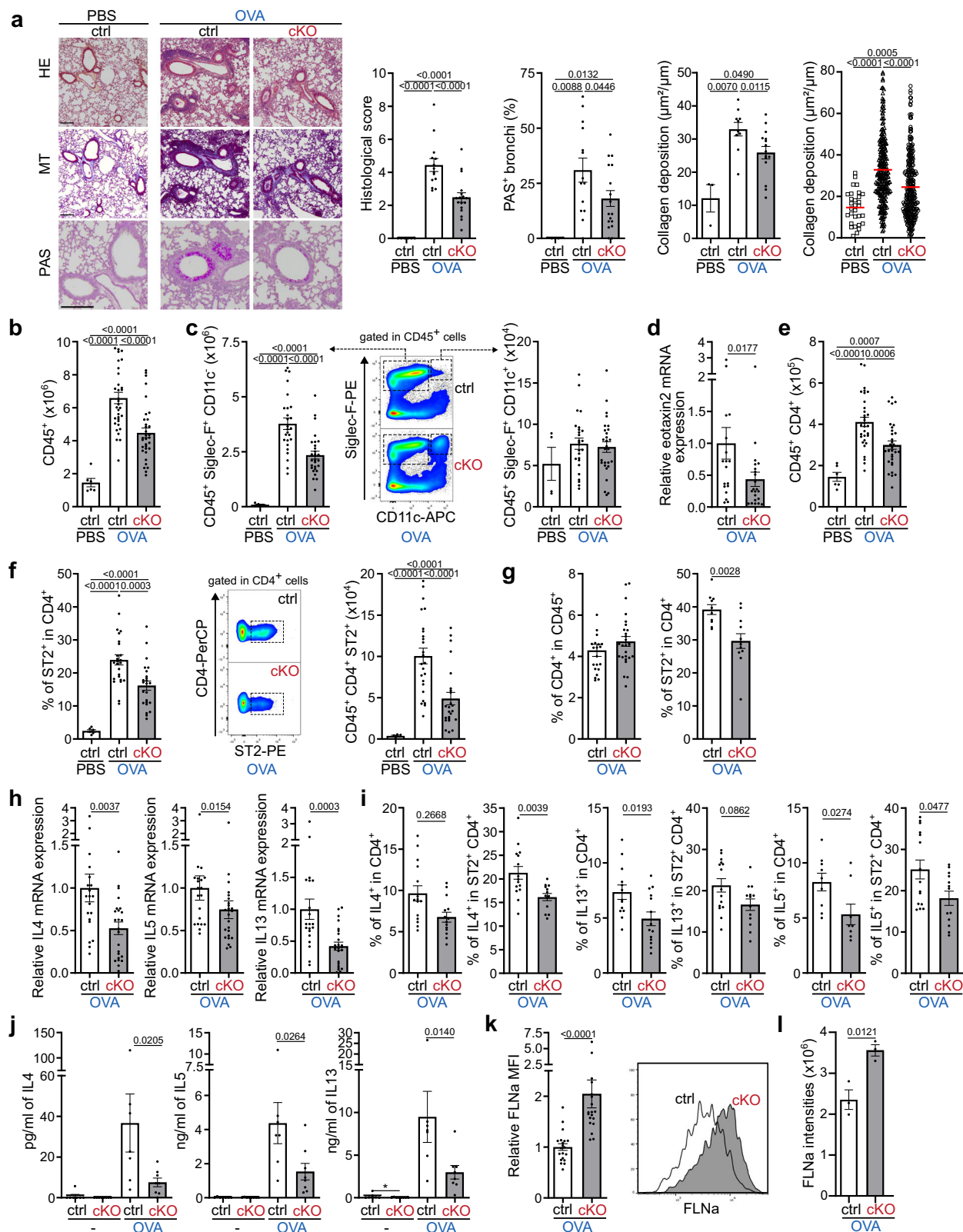
the TCR and the CD28 costimulatory molecule[16–18], our data revealed that the loss of ASB2α has no impact on the transcriptomic program of Th2 lymphocytes. These strongly suggest that the ASB2α-FLNa/FLNb axis is unlikely to play roles in cell signaling and/or transcriptional regulation in Th2 lymphocytes, at least, following TCR/CD28 engagement. Because FLNa plays key roles in the architecture and the mechanics of the actin cytoskeleton[40], our results suggest that low

levels of FLNa and FLNb in Th2 lymphocytes compared to in Th1, Th17, and Treg lymphocytes are likely to confer specific morphological features to Th2 lymphocytes. In line with this, compared to Th1, Th17, and Treg lymphocytes, Th2 lymphocytes harbor an elongated shape that is lost in ASB2α-deficient Th2 lymphocytes. Studies proposed that, in contrast to Th1 lymphocytes, Th2 lymphocytes adopt a fast and wide scanning strategy that depends on $\alpha_V\beta_3$ integrins but is uncoupled

Fig. 6 | Deletion of *ASB2* in hematopoietic cells attenuates OVA-airway inflammation in mice. Ctrl and *ASB2* cKO mice were submitted to OVA-airway inflammation (OVA) as indicated in the online methods. Ctrl mice treated with PBS were used as controls. **a** Inflammation of the lungs assessed using hematoxylin and eosin (HE) staining of lung sections to analyze the infiltration of inflammatory cells (0–12-point scale), Masson's trichrome (MT) staining of lung sections to visualize and quantify collagen deposits ($\mu m^2/\mu m$) (collagen area/bronchus perimeter), and periodic acid Schiff (PAS) staining to visualize and quantify mucus production. **b** Data represents the numbers of CD45$^+$ cells in the lungs. **c** Numbers of CD45$^+$Siglec-F$^+$CD11c$^-$ (eosinophils, left panel) and CD45$^+$Siglec-F$^+$CD11c$^+$ (alveolar macrophages; right panel). Representative flow cytometry plots for CD11c and Siglec-F within a CD45$^+$ gated (middle panel) in the lungs of OVA-treated mice. **d** Relative expression of eotaxin 2 mRNA in the lung lysates assessed by RT-qPCR. **e** Numbers of CD45$^+$CD4$^+$ in the lungs. **f** Percentage of ST2$^+$ cells in CD4$^+$ cells, representative flow cytometry plots for ST2 and CD4 within a CD4$^+$ gate, and numbers of CD45$^+$CD4$^+$ST2$^+$ in the lungs. **g** Data represents the percentage of CD4$^+$ in CD45$^+$ cells and the percentage of ST2$^+$ in CD4$^+$ cells in the BAL fluids. **h** Relative expression of IL-4, IL-5 and IL-13 mRNA in the lung lysates. **i** Data represents the percentage of IL-4$^+$, IL-5$^+$ or IL-13$^+$ in CD4$^+$ cells and in ST2$^+$CD4$^+$ cells in the lungs. **j** Production of IL-4, IL-5, and IL-13 measured by ELISA after antigen restimulation (OVA) or not (−) of cells of the lung draining lymph nodes of mice submitted to OVA-induced airway inflammation. **k** Expression of FLNa was analyzed by intracellular flow cytometry in CD45$^+$CD4$^+$ST2$^+$ cells from the lungs of ctrl or *ASB2* cKO mice submitted to OVA-induced airway inflammation. **l** Intensities of FLNa calculated using MaxQuant quantitative metrics in cell extracts of CD45$^+$CD4$^+$ST2$^+$ living cells sorted from the lungs of control or *ASB2* cKO mice submitted to OVA-induced airway inflammation. Data are mean ± SEM of biological replicates. Sample size: ctrl +PBS = 6, ctrl + OVA = 14, and cKO + OVA = 17 for (**a**) (*histological score*); ctrl+PBS = 3, ctrl + OVA = 14, and cKO + OVA = 17 for (**a**) (*PAS+ bronchi*); ctrl + PBS = 3, ctrl + OVA = 10, and cKO + OVA = 15 for (**a**) (*collagen deposition-left*); ctrl + PBS = 30, ctrl + OVA = 249, and cKO + OVA = 275 for (**a**) (*collagen deposition-right*); ctrl + PBS = 6, ctrl + OVA = 34, and cKO + OVA = 33 for (**b**); ctrl + PBS = 5, ctrl + OVA = 26, and cKO + OVA = 28 for (**c**); ctrl + OVA = 19 and cKO + OVA = 22 for (**d**); ctrl + PBS = 6, ctrl + OVA = 32, and cKO + OVA = 31 for (**e**); ctrl + PBS = 5, ctrl + OVA = 25, and cKO + OVA = 24 for (**f**); ctrl + OVA = 21 and cKO + OVA = 27 for (**g**) (*left*); ctrl + OVA = 10 and cKO + OVA = 12 for (**g**) (*right*); ctrl + OVA = 20 and cKO + OVA = 24 for (**h**); ctrl + OVA = 14 and cKO + OVA = 14 for (**i**) (*left*); ctrl + OVA = 14 and cKO + OVA = 14 for (**i**) (*middle*); ctrl + OVA = 9 and cKO + OVA = 8 for (**i**) (*right*); ctrl + OVA = 7 and cKO + OVA = 8 for (**j**); ctrl + OVA = 20 and cKO + OVA = 19 for (**k**); and ctrl + OVA = 3 and cKO + OVA = 3 for (**l**). *p* values were calculated using the two-sided Mann–Whitney *t*-test. Scale bar, 200 μm. Source data are provided as a Source Data file.

from G protein-coupled receptor signals such as those triggered by chemokines[6,7]. We show here that ASB2α-deficient Th2 lymphocytes exhibited a diminished track displacement length and a diminished mean scanned area, associated with a reduced cell velocity compared to their ctrl Th2 lymphocyte counterparts. Furthermore, we observed decreased in vivo recruitment of ASB2α-deficient Th2 lymphocytes in inflamed lungs of mice submitted to airway inflammation or asthma. These results together with the fact that FLNa bridges the actin cytoskeleton to integrins thereby maintaining them in an inactive state[20] and that FLNa associates with active integrins to inhibit cell migration[24], raise the possibility that the low levels of FLNa and FLNb driven by ASB2α in Th2 lymphocyte favor $\alpha_V\beta_3$ integrin-dependent cell migration to optimize their effector functions. Since compensation by FLNb in the absence of FLNa has been observed[27,41], functions of FLNa in T lymphocytes may have been missed or underestimated in assays using FLNa knockout/knockdown cells[42]. Our data also provide evidences that accumulation of FLNa and FLNb in ASB2α-deficient in Th2 lymphocyte inhibits $\alpha_V\beta_3$ integrin-dependent cell migration by enhancing $\alpha_V\beta_3$ integrin outside-in signaling. In line with these findings, it is tempting to speculate that fine-tuning levels of FLNa and FLNb are critical to optimal $\alpha_V\beta_3$ integrin-dependent cell migration of Th2 lymphocytes.

Insight into the world of ubiquitin has expanded considerably over the past decade and ubiquitin conjugation to proteins is known to be involved in controlling major biological processes. E3 ubiquitin ligases are the critical components of the ubiquitylation cascade owing to their control of the substrate selectivity, making these enzymes attractive targets for therapeutic intervention[43,44]. Our results shed light on the key roles of ubiquitylation processes in controlling Th2 lymphocyte functions and point to E3 ubiquitin ligases as potential therapeutic intervention points for inflammatory diseases. Because Th2 lymphocytes are key drivers of type 2 inflammation, direct targeting of Th2 lymphocytes would be expected to drastically lower the burden of type 2-driven diseases. Therefore, ASB2α and its substrates FLNa and FLNb may represent novel pharmacological targets to mitigate type 2 immunity. Taken together, our data highlight a prominent role for ASB2α-mediated degradation of FLNa and FLNb in Th2 lymphocyte functions and credential the ASB2α-FLNa/b axis as a potential therapeutic opportunity in type 2-high asthma.

Methods

Research complies with all relevant ethical regulations. Mice studies were handled according to the Centre National de la Recherche Scientifique (CNRS) and the Institut national de la santé et de la Recherche

médicale (Inserm) ethical guidelines and approved by the French Ministry ethic committees (CEEA-122 & CEEA-001).

Reagent and antibodies
PS-341 (Euromedex) was prepared in DMSO. Antibodies used are described in Supplementary Table 2.

Mice and models of airway allergic inflammation
All mice were housed under specific pathogen-free conditions. Mice were housed in individually ventilated cage (500 cm^2) with a maximum of 5 mice per cage, at 23–25 °C and 53–54% humidity with a 12 h light: 12 h dark with the lights being ON during the daytime. At the end of the studies, mice were euthanized by cervical dislocation. For mouse models of airway inflammation, mice were 8–14 weeks old. Female *Asb2*$^{fl/fl}$ (control) and VE-cadherin (VEC) -Cre;*Asb2*$^{fl/fl}$ (*ASB2* cKO) transgenic mice were generated previously[25,29]. TCR transgenic OT2 mice were crossed with VEC-Cre;*Asb2*$^{fl/fl}$ to generate female OT2;VEC-Cre;*Asb2*$^{fl/fl}$ or OT2;*Asb2*$^{fl/fl}$ mice. Female C57BL/6 J mice were purchased from Janvier Labs. Control or *ASB2* cKO transgenic mice were immunized by intraperitoneal injection of 100 μg ovalbumin (OVA; Sigma-Aldrich) in alum (2 mg; Sigma-Aldrich) or PBS at day 0 and 7. From days 22 to 26, mice were subjected to five daily OVA (50 μg/day) or PBS inhalation and analyzed at day 28. Control or *ASB2* cKO transgenic mice were subjected to HDM inhalation (10 μg) (Dermatophagoides pteronyssinus, Stallergenes Greer) at day 0. From days 7 to 11, mice were subjected to five daily HDM inhalation (10 μg/day) and analyzed at day 16. For Th2 lymphocyte adoptive transfer experiments, 3×10^6 *ASB2* cKO or ctrl OT2 Th2 lymphocytes were injected intravenously into C57Bl/6 J recipients. Recipient mice received intranasal OVA (50 μg) for 1 or 5 days. Twenty-four hours after the last OVA administration, serum, bronchoalveolar lavage fluid (BALF), lungs, and lung-draining lymph nodes (LDLN) were collected and processed. Lungs were digested for 30 min at 37 °C with 0.25 mg/ml Liberase (Sigma-Aldrich) and 0.5 mg/ml DNAse I (Roche). LDLN were digested for 25 min at 37 °C with 2.5 mg/ml collagenase D (Roche). Single-cell suspensions were used after filtration through a 70-μm strainer.

Histological analyses
Lungs were fixed in 4% paraformaldehyde (Electron Microscopy Sciences) at 4 °C for 24 h, placed in 70% ethanol, and paraffin-embedded. Sections (5 μm) were stained with hematoxylin and eosin (HE), Masson Trichrome (MT), or Periodic Acid Schiff (PAS). Histological disease scores from 0 to 3 were attributed based on the severity of peribronchial, perivascular, and interstitial immune cell infiltration, together
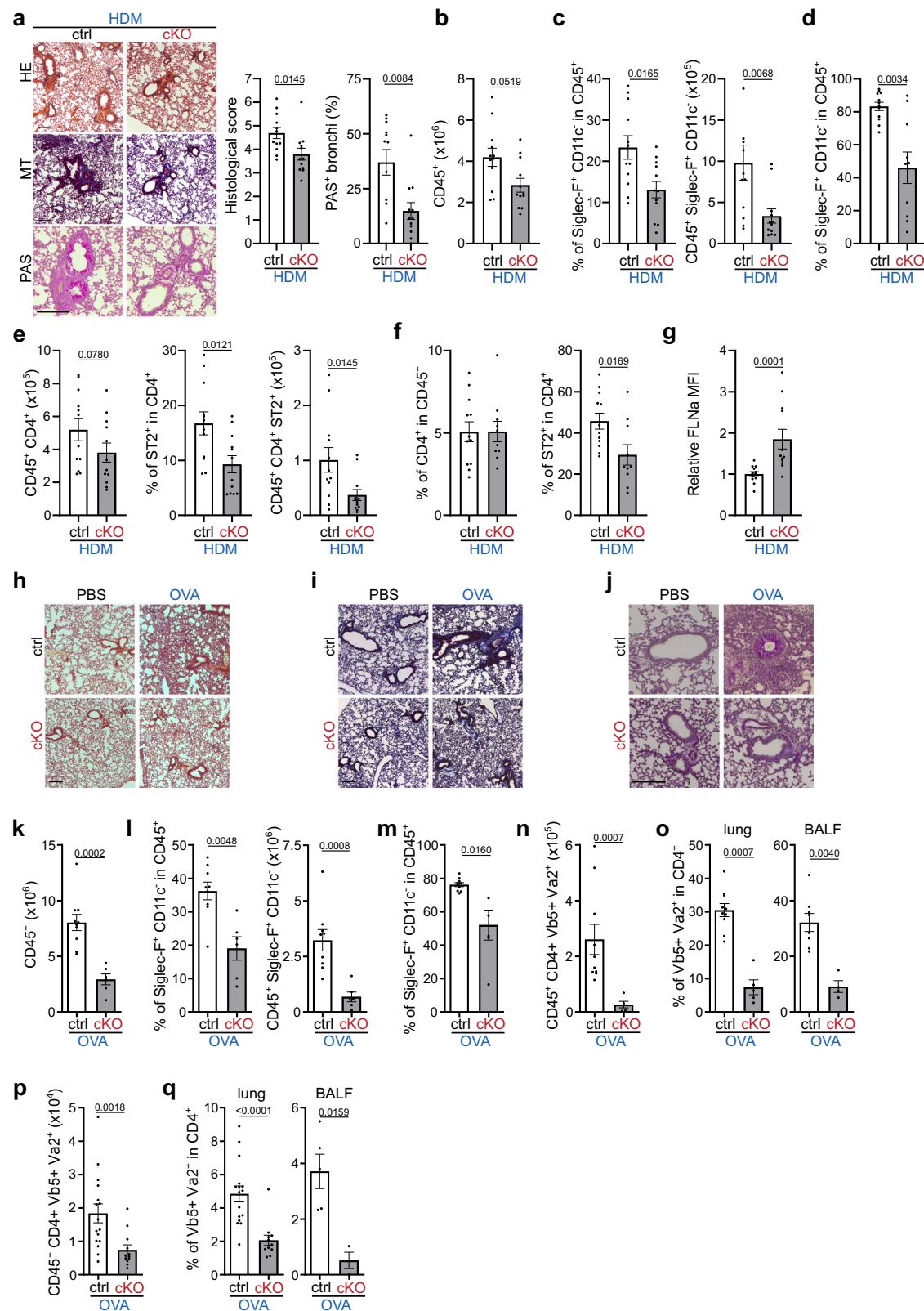
with thickening of peribronchial epithelium, resulting in a maximum score of 12. Collagen deposit and PAS⁺ bronchi were quantified using QuPath version 0.4.1[45]. The algorithm was based on a pixel classifier and was trained on representative pictures with dedicated annotations. Bronchi were manually delineated and the respective total amount of detected collagen was obtained. The percentage of PAS⁺ bronchi was calculated by comparing the percentage of PAS staining in manually detected respective bronchi.

Human peripheral blood mononuclear cells (PBMC)

PBMCs were obtained from Etablissement Français du Sang, and all human participants provided written informed consent, with

Fig. 7 | Deletion of *ASB2* in hematopoietic cells attenuates HDM-asthma in mice and intrinsic loss of *ASB2* in Th2 cells is sufficient to impede airway inflammation. a–g Ctrl and *ASB2* cKO mice were submitted to HDM-allergic airway inflammation (HDM) as indicated. **a** HE, MT, and PAS staining of lung sections to analyze the infiltration of inflammatory cells and inflammatory scores. **b** Data represents the numbers of CD45+ cells in the lungs. **c** Data represents the numbers and the percentages of Siglec-F+CD11c− in CD45+ cells in the lungs. **d** Data represents the percentages of Siglec-F+CD11c− in CD45+ cells in the BAL fluids. **e** Data represents the numbers of CD4+CD45+ cells, the percentages of ST2+ in CD4+ cells, and the numbers of ST2+CD4+CD45+ cells in the lungs. **f** Data represents the percentages of CD4+ in CD45+ cells and the percentages of ST2+ in CD4+ cells in the BAL fluids. **g** Expression of FLNa was analyzed by intracellular flow cytometry in CD45+CD4+ST2+ cells from the lungs of ctrl or *ASB2* cKO mice submitted to HDM-induced asthma. **h–q** OVA-specific Th2 lymphocytes generated from control or *ASB2* cKO OT2 mice were transferred to C57Bl/6 recipients that were subsequently submitted to daily OVA inhalations to induce airway inflammation. Analysis was performed 24 h after the 5th (**H**, **O**) or after the 1st OVA inhalation (**p**, **q**). **h** HE staining of lung sections. **i** MT staining of lung sections. **j** PAS staining of lung sections. **k** Data represents the numbers of CD45+ in the lungs. **l** Data represents the numbers and the percentages of Siglec-F+CD11c− in CD45+ cells in the lungs. **m** Data represents the percentages of Siglec-F+CD11c− in CD45+ cells in the BAL fluids. **n** Data represents the numbers of Vβ5+Vα2+CD4+CD45+ cells in the lungs. **o** Data represents the percentages of Vβ5+Vα2+ in CD4+ cells in the lungs and the BAL fluids. **p** Data represents the numbers of Vβ5+Vα2+CD4+CD45+ cells in the lungs. **q** Data represents the percentages of Vβ5+Vα2+ in CD4+ cells in the lungs and the BAL fluids. Data are mean ± SEM of biological replicates. Sample size: ctrl = 12 and cKO = 12 for (**a–c**); ctrl = 12 and cKO = 10 for (**d**); ctrl = 12 and cKO = 12 for (**e**); ctrl = 12 and cKO = 10 for (**f**); ctrl = 12 and cKO = 12 for (**g**); ctrl = 10 and cKO = 6 for (**k**); ctrl = 9 and cKO = 6 for (**l**); ctrl = 10 and cKO = 6 for (**m**, **n**); ctrl = 10 and cKO = 6 for (**o**) (left); ctrl = 8 and cKO = 4 for (**o**) (*right*); ctrl = 16 and cKO = 12 for (**p**); ctrl = 16 and cKO = 12 for (**q**) (*left*); and ctrl = 5 and cKO = 4 for (**q**) (*right*). *p* values were calculated using the two-sided Mann–Whitney *t*-test. Scale bar, 200 μm. Source data are provided as a Source Data file.

appropriate ethical permission in place. Eight healthy individuals (age from 21- to 43-year-old) were enrolled in this study.

T lymphocyte culture

Mouse naive CD4+ cells were isolated from spleen immunocytes of mice using a CD4 naive T-cell Isolation Kit (#480040; BioLegend) and stimulated for 3 days with plate-bound anti-CD3ε (5 μg/ml) and were differentiated in the presence of polarizing cytokines and antibody cocktails (Th1: 10 ng/ml IL-2, 10 ng/ml IL-12, 2 μg/ml anti-CD28, and 10 μg/ml anti-IL-4; Th2: 10 ng/ml IL-2, 20 ng/ml IL-4, 1 μg/ml anti-CD28, and 10 μg/ml anti-IFNγ; Treg: 10 ng/ml IL-2, 3 ng/ml TGFβ, and 2 μg/ml anti-CD28; and Th17: 2 ng/ml TGFβ, 20 ng/ml IL-6, 10 ng/ml IL-23, 10 ng/ml IL-1β, 1 μg/ml anti-CD28, 6 μg/ml anti-IFNγ, and 10 μg/ml anti-IL-4) in RPMI containing 10% FCS, 1% glutamine, 0.1% β-mercaptoethanol, and 1% penicillin/streptomycin in 24-well plates. For Th2 lymphocyte adoptive transfer experiments, purified naive OT2 CD4+ T lymphocytes were stimulated with irradiated splenocytes (24 Gy) and OVA peptide (323–339) (Sigma-Aldrich) in culture medium supplemented with 10 ng/ml IL-2, 20 ng/ml IL-4, 1 μg/ml anti-CD28 and 10 μg/ml anti-IFNγ. Cells were then split on noncoated plates and cultured for 3 additional days in fresh differentiating medium without antibodies (Th1: 20 ng/ml IL-2 and 10 ng/ml IL-12; Th2: 20 ng/ml IL-2 and 20 ng/ml IL-4; Treg: 20 ng/ml IL-2 and 3 ng/ml TGFβ1; and Th17: 10 ng/ml IL-2, 2 ng/mL TGFβ1, 20 ng/ml IL-6, 10 ng/ml IL-23, and 10 ng/mL IL-1β). Recombinant mouse cytokines were from Miltenyi Biotec (IL-2, IL-4, IL-6, IL-1β, and IL-23) and PeproTech (IL-12). TGFβ was from Active Bioscience. For RNA-seq analysis, Th2 lymphocytes were stimulated at day 5 with 3 μg/ml coated anti-CD3ε and 2 μg/ml soluble anti-CD28 for 24 h. Naive human CD4+ T lymphocytes were isolated from PBMCs using a CD4 naive T-cell Isolation Kit (#480042; BioLegend). In Vitro, differentiation of human Th1 and Th2 lymphocytes was performed using the CellXVivo Human Th1 Cell Differentiation Kit (#CDK001) and the CellXVivo Human Th2 Cell Differentiation Kit (#CDK002), respectively, as recommended by the manufacturer (Biotechne). Freshly thawed PBMCs were cultured in RPMI 1640 supplemented with 5% FBS, 1 mM sodium pyruvate, 2 mM glutamine, 100 U/ml penicillin, 100 mg/ml streptomycin, 1 mM HEPES, and 1% NEAA medium for 24 h before analyses.

ELISA

Lung draining lymph node cells were seeded into 96-well flat-bottom plates (6×10^5 cells per well) and stimulated with 200 μg/ml ovalbumin in complete medium (RPMI 1640 supplemented with 10% FBS, 1% pyruvate, 2 mM glutamine, 100 U/ml penicillin, 100 mg/ml streptomycin, and 50 μM β-mercaptoethanol) for 72 h, and cytokine production was quantified by ELISA according to the manufacturer (Invitrogen).

RT-qPCR

Total RNA was extracted with the NucleoSpin RNA kit (#740955; Macherey-Nagel) (cDNA was synthesized using the OneScript Plus cDNA Synthesis Kit G236) as recommended by the manufacturer (Applied Biological Materials). Real-time PCR was carried out with the LC480 real-time PCR system (Roche Diagnostics) using the BlasTaq 2X qPCR MasterMix (G892) (Applied Biological Materials) according to the manufacturer's instructions. Data were analyzed using the Light-Cycler 480 software (v1.5.1.62). The specificity of the PCR primers was confirmed by melting curve analyses. Gene expression was determined using the ΔΔCt method and data are presented as relative amounts of mRNA normalized to Rplp0 (ribosomal protein, large, P0) or YWHAZ for mouse or human cells, respectively. The primers used for qPCR are shown in Supplementary Table 1.

Micro-array and chromatin immunoprecipitation sequencing analysis

Micro-array data of *ASB2* expression in naive human CD4+ T lymphocytes or cells cultured under Th2 conditions were retrieved from the a GSE60680[46]. Data of RNA-seq and ChIP-seq of H3K27ac, H3K4me1, H3K27me3, and RNA polymerase II in naive CD4+ T lymphocytes or in T lymphocytes cultured under Th1, Th2, and Th17 conditions were retrieved from the GSE144586 dataset[30]. The genomic tracks around candidate loci were generated using pyGenomeTracks (v3.8) and the expression heatmap with pheatmap R package (v1.0.12). Micro-array *ASB2*, *ITGAV*, and *ITGB3* expression data in OVA-induced airway inflammation and HDM-induced asthma were retrieved from the publicly available GSE109737[31] and GSE72005[32] datasets, respectively.

RNA-seq

Total RNA was extracted with the Nuclespin RNA kit (Macherey-Nagel) and subsequently used to prepare the libraries using the Stranded Total RNA Prep, Ligation with Ribo-Zero Plus kit (Illumina). Quality controls of the libraries were performed using standard methods, including quantification with Qubit spectrophotometer and assessment of size distribution with TapeStation 4150 (Agilent). Samples were indexed and sequenced (paired-end reads of 150 bp) on the NovaSeq 6000 system (Illumina) from the Genomic and Transcriptomic Platform of the GeT core facility (Toulouse, France). Raw sequencing reads were processed using nf-core/RNAseq pipeline v.3.12.0 developed with Nextflow[47,48]. Briefly, this pipeline trims adapters and removes low-quality reads using Cutadapt v.3.4[49]. It then aligns reads to the Ensemble GRCm39_v.107 genome using STAR v.2.7.9a[50]. Finally, gene expression was quantified with Salmon v.1.10.1[51]. Only samples with more than 10 M reads were kept for further analyses. Raw counts were normalized and differential expression analyses were performed using the R package DESeq2 v.1.38.3[52].

Differentially expressed genes between activated and non-activated ctrl Th2 lymphocytes were identified as genes with an adjusted p value below 0.5 and an absolute log2 fold change greater than 2. Gene Set Enrichment analyses were performed with ClusterProfiler v.4.6.2[53,54]. Heatmap and boxplots were made using Th1 and Th2 genve sets extracted from[55] and Th17 gene set extracted from the Harmonizome database v.3.0[56]. RNA-seq data used in this study have been deposited at GEO under accession number GSE251847.

Flow cytometry

For flow cytometry analysis and cell sorting, cells were first incubated with Zombie viability dyes (BioLegend) for 15 min at room temperature and then incubated for 30 min a 4 °C with the appropriate combination of antibodies. IL-4, IL-5, IL-13, and IFNγ were measured by intracellular staining after stimulation for 4 h with phorbol 12-myristate 13-acetate (50 ng/ml, Sigma-Aldrich), ionomycin (500 ng/ml, Sigma-Aldrich) and Monensin (BioLegend). Cells were fixed after extracellular staining with PBS 4% PFA 20 min at 4 °C and permeabilized by adding PBS 0.5% Triton X100 10 min at 4 °C. For quantification of FLNa expression by flow cytometry, cells were fixed with Fixation/Permeabilization buffer (Invitrogen) overnight at 4 °C and were then immunostained with anti-FLNa and Alexa Fluor 488-conjugated goat anti-rabbit antibodies (Invitrogen) in Permeabilization buffer (Invitrogen). Flow cytometry analysis was performed with LSRII or Fortessa X20 Cytometers (BD Biosciences) and cell sorting on a FACS ARIA II Cytometer (BD Biosciences). Analyses of flow cytometry data were performed using FlowJo (TreeStar; v10.8.1). FACS sequential gating or sorting strategies are shown in Supplementary Fig. 5-8.

High-content imaging, image acquisition, and processing

CellCarrier Ultra tissue culture treated 384-well plates (Perkin Elmer) were coated with 1 μg/ml vitronectin (BioLegend) or 1 μg/ml of VCAM-1 (BioLegend). Ten thousand human naive CD4$^+$ or Th2 lymphocytes or mouse Th1, ctrl Th2, *ASB2* cKO Th2, Treg, or Th17 cells were seeded per well and incubated 25 min at 37 °C to adhere in RPMI 1640 supplemented with 10% FBS, 2 mM glutamine, 100 U/mL penicillin and 100 mg/mL streptomycin and then fixed with 4% paraformaldehyde, 60 mM sucrose (Sigma-Aldrich). After fixation, cells were washed and stained with anti-FLNa, anti-FLNb, and phalloidin. Nuclei were stained with 50 ng/ml of DAPI. Images were acquired on an automated Opera Phenix confocal HCS device (Perkin Elmer) with a 40 × 1.1 NA Plan Apochromat water immersion objective and a SCMOS camera. Thirteen non-adjacent fields and 3 stacks per field (1 μm step) were acquired per well. Stacks of images were combined, then assembled in sets of images per field of view corresponding to DAPI, phalloidin, FLNa, and/or FLNb. These datasets were processed, and measurements were made using the Harmony software.

Time-lapse imaging and analyses

Six channel μ-slide VI 0.4 (Ibidi) were coated overnight with 1 μg/ml of vitronectin (BioLegend). Control, *ASB2* cKO, and ctrl Th2 lymphocytes were labeled 15 min at 37 °C with 0.6 μM CellTracker Green (CTG) CMFDA (Invitrogen) in HBSS without Ca^{2+} and Mg^{2+}. Labeling reactions were stopped by addition of HBSS without Ca^{2+} and Mg^{2+}. 8×10^4 Th2 lymphocytes in 0.1 ml RPMI medium containing 1% BSA and 10 mM HEPES were seeded per well and migration was initiated by the addition of 10% FBS. When indicated Th2 lymphocytes were treated with 0.5 mM MnCl$_2$ and a combination of 0.2 μg/ml of antibodies against mouse CD51 (Clone RMV-7) or the corresponding isotypic controls (Clone HTK888), and 0.2 μg/ml of antibodies against mouse CD61 (Clone 2C9.G2) or the corresponding isotypic controls (Clone HTK888). The microscope environmental chamber was maintained and monitored at 37 °C and 5% CO$_2$. Images were acquired by spinning disk confocal microscopy (Yogokawa head, Hamamatsu CMOS Flash4 camera, 20× objective NA 0.75) using the Metamorph

v7.10.1.161 software. Images were acquired every minute for both transmitted light and 491 nm CTG-associated fluorescence. Multiple parameters measurements of images were performed via IMARIS v10.0.1 software (Oxford Instruments). Distance and directionality data were obtained using spot function. Shape description data were obtained using surface function. Spider plots were obtained using the MatLab (Mathworks, R2009a, v7.10) algorithm and IMARIS Translate Tracks Xtension on track distance data. Supplementary videos were encoded at 10 frames/s.

Western blot

For immunoblot analysis, cells were pelleted, washed in PBS, and lysed using in whole-cell extract buffer containing 50 mM Tris-HCl (pH 7.9), 150 mM NaCl, 1 mM EDTA, 0.1% Igepal CA-630, 10% glycerol, 1 mM dithiothreitol, 1 mM Na$_3$VO$_4$, 50 mM NaF, 25 mM β glycerophosphate, 2 mM Na pyrophosphate and 1% protease inhibitor cocktail (P8340; Sigma-Aldrich). After three freeze-thaw cycle in liquid nitrogen, the resulting cell lysates were cleared by a 20 min 20,000 × g centrifugation at 4 °C. The lysates were boiled with Laemmli buffer, resolved by SDS–polyacrylamide gel electrophoresis, transferred to nitrocellulose membranes, and the proteins visualized by standard immunoblotting procedures. Signal acquisition was conducted using the Bio-Rad ChemiDoc apparatus and quantification of the immunoblot signal was performed with the Bio-Rad Image Lab v6.1 software. Protein quantifications were normalized to the levels of the GAPDH protein.

Immunoprecipitation

Ctrl and *ASB2* cKO Th2 lymphocytes generated in vitro from naive CD4+ T lymphocytes were washed twice in ice-cold PBS, and lysed in Triton X100 lysis buffer containing 20 mM Tris-HCl, pH 8, 137 mM NaCl, 10% glycerol and 1% Triton X100 and supplemented with 1% protease inhibitor cocktail (Sigma-Aldrich), 1 mM DTT, 1 mM Na$_3$VO$_4$, 50 mM NaF, 2 mM sodium pyrophosphate and 25 mM β-glycerophosphate. After a 30 min incubation on ice, cell lysates were cleared by a 20-min 20,000 × g centrifugation at 4 °C. 100 μg ctrl or *ASB2* cKO Th2 lymphocyte extracts was precleared by incubating 30 min in the presence of protein A-Sepharose beads (Cytiva) in a binding buffer containing 20 mM Tris-HCl pH 8, 250 mM NaCl, 10% glycerol and 0.1% Igepal CA-630 at 4 °C. Anti-rabbit FLNa serum or rabbit pre-immune serum was added to the precleared cell extracts. After 16 h of incubation, immunocomplexes were recovered with protein A-Sepharose. After three washes with binding buffer, proteins were eluted with boiling Laemmli's buffer, fractionated by SDS-polyacrylamide gel electrophoresis (SDS-PAGE), and analyzed by immunoblotting with anti-FLNa. After incubation with the Restore western blot stripping buffer (Fisher Scientific), proteins were probed with antibodies to ubiquitylated proteins.

Proteome analysis

Ctrl and *ASB2* cKO Th2 lymphocytes generated in vitro from naive CD4$^+$ T lymphocytes and CD45$^+$CD4$^+$ST2$^+$ living cells sorted from the lungs of control or *ASB2* cKO mice submitted to OVA-induced airway inflammation were lysed in 5% SDS, 50 mM ammonium bicarbonate and sonicated on a Bioruptor (Diagenode). Proteins were digested on S-trap devices (Protifi) and 50 ng of the resulting peptides were analyzed by nanoLC-MS/MS using an UltiMate 3000 RS nanoLC system (ThermoFisher Scientific) coupled to a TIMS-TOF SCP mass spectrometer (Bruker). Peptides were separated on a C18 Aurora column (25 cm × 75 μm ID, IonOpticks) using a gradient ramping from 2% to 20% of B in 30 min, then to 37% of B in 3 min and to 85% of B in 2 min (solvent A: 0.1% FA in H$_2$O; solvent B 0.1% FA in acetonitrile), with a flow rate of 150 nl/min. MS acquisition was performed in DIA-PASEF mode on the precursor mass range [400–1000] m/z and ion mobility 1/K0 [0.64–1.37]. The acquisition scheme was composed of 8 consecutive TIMS ramps using an accumulation time of 100 ms, with 3 MS/MS

acquisition windows of 25 Th for each of them. The resulting cycle time was 0.96 s. The collision energy was ramped linearly as a function of the ion mobility from 59 eV at $1/K0 = 1.6$ Vs cm^{-2} to 20 eV at $1/K0 = 0.6$ Vs cm^{-2}. Nine independent replicate samples for each condition (ctrl or *ASB2* cKO), obtained from two different cell culture experiments, were analyzed in total. The raw data (18 files) was searched and quantified with DIA-NN 1.8.1, using a predicted library generated by the software from the UniProt mouse reference proteome. Validation was performed at 1% precursor and protein FDR, with a peptide length range set at 7–30 and precursor charge range set at 2–3. MS intensities measured by DIA-NN for each peptide ions (precursor matrix) were processed using the Proline software[57] for calculation of protein intensities (peptide-to-protein inference and summarization of peptide intensities) and normalization. Only proteins detected and quantified in more than 2 replicates from at least one of the conditions (ctrl or *ASB2* cKO), and quantified based on more than 2 peptides, were kept for statistical analysis. Normalized abundance values were log2-transformed, and missing values were imputed with a low-intensity value reflecting the noise background, defined for each analytical run as the lowest 1% percentile value of the total protein intensity distribution. A student *t*-test (bilateral, equal variance) was calculated based on the 9 replicates to evaluate statistical significance of the protein abundance variation between the two conditions. The MS proteomics data have been deposited to the ProteomeXchange Consortium via the PRIDE[58] partner repository with the dataset identifier PXD044062.

Statistical analyses

All *p* values were calculated using the nonparametric Mann–Whitney *t*-test except in Fig. 1g, j, m, and in Fig. 3d where the Wilcoxon's test was used. For the proteome analyses, the Student *t*-test was used in the statistical analysis. In Fig. 4h, i, correlations between nonparametric variables were evaluated using Spearman rank correlation test (r).

Reporting summary

Further information on research design is available in the Nature Portfolio Reporting Summary linked to this article.

Data availability

The MS proteomics data generated in this study have been deposited to the ProteomeXchange Consortium via the PRIDE partner repository with the dataset identifier PXD044062. The RNA-seq data from this study have been deposited at GEO under accession number GSE251847. Data of RNA-seq and ChIP-seq from publicly accessible datasets were retrieved from GSE60680, GSE144586, GSE109737, and GSE72005. All other data are available in the article and its Supplementary files or from the corresponding authors upon request. Source data are provided with this paper.

References

1. Muehling, L. M., Lawrence, M. G. & Woodfolk, J. A. Pathogenic CD4(+) T cells in patients with asthma. *J. Allergy Clin. Immunol.* **140**, 1523–1540 (2017).
2. Vieira Braga, F. A. et al. A cellular census of human lungs identifies novel cell states in health and in asthma. *Nat. Med.* **25**, 1153–1163 (2019).
3. Gandhi, N. A. et al. Targeting key proximal drivers of type 2 inflammation in disease. *Nat. Rev. Drug Discov.* **15**, 35–50 (2016).
4. Kolkhir, P. et al. Type 2 chronic inflammatory diseases: targets, therapies and unmet needs. *Nat. Rev. Drug Discov.* **22**, 743–767 (2023).
5. Krummel, M. F., Bartumeus, F. & Gérard, A. T cell migration, search strategies and mechanisms. *Nat. Rev. Immunol.* **16**, 193–201 (2016).
6. Overstreet, M. G. et al. Inflammation-induced interstitial migration of effector CD4(+) T cells is dependent on integrin alphaV. *Nat. Immunol.* **14**, 949–958 (2013).
7. Gaylo-Moynihan, A. et al. Programming of distinct chemokine-dependent and -independent search strategies for Th1 and Th2 cells optimizes function at inflamed sites. *Immunity* **51**, 298–309.e6 (2019).
8. Layman, A. A. & Oliver, P. M. Ubiquitin ligases and deubiquitinating enzymes in CD4+ T cell effector fate choice and function. *J. Immunol.* **196**, 3975–3982 (2016).
9. Gao, S. F., Zhong, B. & Lin, D. Regulation of T helper cell differentiation by E3 ubiquitin ligases and deubiquitinating enzymes. *Int. Immunopharmacol.* **42**, 150–156 (2017).
10. Heuze, M. L. et al. ASB2 is an Elongin BC-interacting protein that can assemble with Cullin 5 and Rbx1 to reconstitute an E3 ubiquitin ligase complex. *J. Biol. Chem.* **280**, 5468–5474 (2005).
11. Horiuchi, S. et al. Genome-wide analysis reveals unique regulation of transcription of Th2-specific genes by GATA3. *J. Immunol.* **186**, 6378–6389 (2011).
12. Sasaki, T. et al. Genome-wide gene expression profiling revealed a critical role for GATA3 in the maintenance of the Th2 cell identity. *PLoS ONE* **8**, e66468 (2013).
13. Spinner, C. A. et al. The E3 ubiquitin ligase Asb2alpha in T helper 2 cells negatively regulates antitumor immunity in colorectal cancer. *Cancer Immunol. Res.* **7**, 1332–1344 (2019).
14. Heuze, M. L. et al. ASB2 targets filamins A and B to proteasomal degradation. *Blood* **112**, 5130–5140 (2008).
15. Nakamura, F., Osborn, T. M., Hartemink, C. A., Hartwig, J. H. & Stossel, T. P. Structural basis of filamin A functions. *J. Cell Biol.* **179**, 1011–1025 (2007).
16. Tavano, R. et al. CD28 interaction with filamin-A controls lipid raft accumulation at the T-cell immunological synapse. *Nat. Cell Biol.* **8**, 1270–1276 (2006).
17. Hayashi, K. & Altman, A. Filamin A is required for T cell activation mediated by protein kinase C-theta. *J. Immunol.* **177**, 1721–1728 (2006).
18. Wang, X. D. et al. TCR-induced sumoylation of the kinase PKC-theta controls T cell synapse organization and T cell activation. *Nat. Immunol.* **16**, 1195–1203 (2015).
19. Grimbert, P. et al. The Filamin-A is a partner of Tc-mip, a new adapter protein involved in c-maf-dependent Th2 signaling pathway. *Mol. Immunol.* **40**, 1257–1261 (2004).
20. Lamsoul, I., Dupré, L. & Lutz, P. G. Molecular tuning of filamin A activities in the context of adhesion and migration. *Front. Cell Dev. Biol.* **8**, 591323 (2020).
21. Kiema, T. et al. The molecular basis of filamin binding to integrins and competition with talin. *Mol. Cell* **21**, 337–347 (2006).
22. Ithychanda, S. S. et al. Identification and characterization of multiple similar ligand-binding repeats in filamin: implication on filamin-mediated receptor clustering and cross-talk. *J. Biol. Chem.* **284**, 35113–35121 (2009).
23. Liu, J. et al. Structural mechanism of integrin inactivation by filamin. *Nat. Struct. Mol. Biol.* **22**, 383–389 (2015).
24. Liu, J. et al. A mechanism of platelet integrin αIIbβ3 outside-in signaling through a novel integrin αIIb subunit–filamin–actin linkage. *Blood* **141**, 2629–2641 (2023).
25. Métais, A. et al. Asb2α-filamin a axis is essential for actin cytoskeleton remodeling during heart development. *Circ. Res.* **122**, e34–e48 (2018).
26. Burande, C. F. et al. A label-free quantitative proteomics strategy to identify E3 ubiquitin ligase substrates targeted to proteasome degradation. *Mol. Cell. Proteom.* **8**, 1719–1727 (2009).
27. Baldassarre, M. et al. Filamins regulate cell spreading and initiation of cell migration. *PLoS ONE* **4**, e7830 (2009).

28. Lamsoul, I. et al. Functional and structural insights into ASB2α, a novel regulator of integrin-dependent adhesion of hematopoietic cells. *J. Biol. Chem.* **286**, 30571–30581 (2011).

29. Lamsoul, I. et al. ASB2α regulates migration of immature dendritic cells. *Blood* **122**, 533–541 (2013).

30. Maqbool, M. A. et al. Alternative enhancer usage and targeted polycomb marking hallmark promoter choice during T cell differentiation. *Cell Rep.* **32**, 108048 (2020).

31. Kilic, A. et al. A systems immunology approach identifies the collective impact of 5 miRs in Th2 inflammation. *JCI Insight* **3**, e97503 (2018).

32. Coquet, J. M. et al. Interleukin-21-producing CD4(+) T cells promote type 2 immunity to house dust mites. *Immunity* **43**, 318–330 (2015).

33. Wei, G. et al. Genome-wide analyses of transcription factor GATA3-mediated gene regulation in distinct T cell types. *Immunity* **35**, 299–311 (2011).

34. Kuwahara, M. et al. Bach2-Batf interactions control Th2-type immune response by regulating the IL-4 amplification loop. *Nat. Commun.* **7**, 12596 (2016).

35. Iwata, A. et al. Quality of TCR signaling determined by differential affinities of enhancers for the composite BATF-IRF4 transcription factor complex. *Nat. Immunol.* **18**, 563–572 (2017).

36. Wei, G. et al. Global mapping of H3K4me3 and H3K27me3 reveals specificity and plasticity in lineage fate determination of differentiating CD4+ T cells. *Immunity* **30**, 155–167 (2009).

37. Endo, Y. et al. Eomesodermin controls interleukin-5 production in memory T helper 2 cells through inhibition of activity of the transcription factor GATA3. *Immunity* **35**, 733–745 (2011).

38. Tibbitt, C. A. et al. Single-cell RNA sequencing of the T helper cell response to house dust mites defines a distinct gene expression signature in airway Th2 cells. *Immunity* **51**, 169–184.e5 (2019).

39. Szeto, A. C. H. et al. An αvβ3 integrin checkpoint is critical for efficient TH2 cell cytokine polarization and potentiation of antigen-specific immunity. *Nat. Immunol.* **24**, 123–135 (2022).

40. Razinia, Z., Makela, T., Ylanne, J. & Calderwood, D. A. Filamins in mechanosensing and signaling. *Annu. Rev. Biophys.* **41**, 227–246 (2012).

41. Sheen, V. L. et al. Filamin A and Filamin B are co-expressed within neurons during periods of neuronal migration and can physically interact. *Hum. Mol. Genet.* **11**, 2845–2854 (2002).

42. Savinko, T. et al. Filamin A is required for optimal T cell integrin-mediated force transmission, flow adhesion, and T cell trafficking. *J. Immunol.* **200**, 3109–3116 (2018).

43. Skaar, J. R., Pagan, J. K. & Pagano, M. SCF ubiquitin ligase-targeted therapies. *Nat. Rev. Drug Discov.* **13**, 889–903 (2014).

44. Lamsoul, I., Uttenweiler-Joseph, S., Moog-Lutz, C. & Lutz, P. G. Cullin 5-RING E3 ubiquitin ligases, new therapeutic targets? *Biochimie* **122**, 339–347 (2016).

45. Bankhead, P. et al. QuPath: open-source software for digital pathology image analysis. *Sci. Rep.* **7**, 1–7 (2017).

46. Gustafsson, M. et al. A validated gene regulatory network and GWAS identifies early regulators of T cell-associated diseases. *Sci. Transl. Med.* **7**, 1–10 (2015).

47. Ewels, P. A. et al. The nf-core framework for community-curated bioinformatics pipelines. *Nat. Biotechnol.* **38**, 276–278 (2020).

48. DI Tommaso, P. et al. Nextflow enables reproducible computational workflows. *Nat. Biotechnol.* **35**, 316–319 (2017).

49. Martin, M. Cutadapt removes adapter sequences from high-throughput sequencing reads. *EMBnet. J.* **17**, 10–12 (2011).

50. Dobin, A. et al. STAR: ultrafast universal RNA-seq aligner. *Bioinformatics* **29**, 15–21 (2013).

51. Patro, R., Duggal, G., Love, M. I., Irizarry, R. A. & Kingsford, C. Salmon provides fast and bias-aware quantification of transcript expression. *Nat. Methods* **14**, 417–419 (2017).

52. Love, M. I., Huber, W. & Anders, S. Moderated estimation of fold change and dispersion for RNA-seq data with DESeq2. *Genome Biol.* **15**, 550 (2014).

53. Wu, T. et al. ClusterProfiler 4.0: a universal enrichment tool for interpreting omics data. *Innovation* **2**, 100141 (2021).

54. Yu, G., Wang, L.-G., Han, Y. & He, Q.-Y. clusterProfiler: an R package for comparing biological themes among gene clusters. *OMICS* **16**, 284–287 (2012).

55. Adoue, V. et al. The histone methyltransferase SETDB1 controls T helper cell lineage integrity by repressing endogenous retroviruses. *Immunity* **50**, 629–644.e8 (2019).

56. Rouillard, A. D. et al. The harmonizome: a collection of processed datasets gathered to serve and mine knowledge about genes and proteins. *Database* **2016**, baw100 (2016).

57. Bouyssié, D. et al. Proline: an efficient and user-friendly software suite for large-scale proteomics. *Bioinformatics* **36**, 3148–3155 (2020).

58. Perez-Riverol, Y. et al. The PRIDE database resources in 2022: a hub for mass spectrometry-based proteomics evidences. *Nucleic Acids Res.* **50**, D543–D552 (2022).

Acknowledgements

Author contributions

P.G.L and I.L. devised, performed, analyzed, interpreted experiments, and wrote the paper. K.M., L.C., M.C-L., C.B., A.M., L. F-V., and H.T. performed, analyzed, and interpreted experiments. Proteomic analyses were coordinated by A.G.P. performed and analyzed by L.C-S. Epigenetic analyses were coordinated by O.J. performed, and analyzed by S.G., A.C., and M.Z., M.S., and A.S. contributed important ideas. Funding was acquired by P.G.L. and I.L. All authors provided critical input into the manuscript.

Competing interests

Additional information

Supplementary information The online version contains supplementary material available at https://doi.org/10.1038/s41467-024-53768-3.

Correspondence and requests for materials should be addressed to Pierre G. Lutz or Isabelle Lamsoul.

Peer review information *Nature Communications* thanks Loretta Tuosto and the other, anonymous, reviewer(s) for their contribution to the peer review of this work. A peer review file is available.

Reprints and permissions information is available at http://www.nature.com/reprints

Publisher's note Springer Nature remains neutral with regard to jurisdictional claims in published maps and institutional affiliations.